Published online: March 7, 2016

Article

SOURCE DATA | TRANSPARENT PROCESS | OPEN ACCESS

THE EMBO JOURNAL

Toxic gain of function from mutant FUS protein is crucial to trigger cell autonomous motor neuron loss

Jelena Scekic-Zahirovic[1,2], Oliver Sendscheid[3,4], Hajer El Oussini[1,2], Mélanie Jambeau[5,6], Ying Sun[5,6], Sina Mersmann[3,4], Marina Wagner[3,4], Stéphane Dieterlé[1,2], Jérome Sinniger[1,2], Sylvie Dirrig-Grosch[1,2], Kevin Drenner[5,6], Marie-Christine Birling[7], Jinsong Qiu[8], Yu Zhou[8], Hairi Li[8], Xiang-Dong Fu[8], Caroline Rouaux[1,2], Tatyana Shelkovnikova[9], Anke Witting[10], Albert C Ludolph[10], Friedemann Kiefer[11], Erik Storkebaum[3,4,*], Clotilde Lagier-Tourenne[5,6,†,**] & Luc Dupuis[1,2,***]

Abstract

FUS is an RNA-binding protein involved in amyotrophic lateral sclerosis (ALS) and frontotemporal dementia (FTD). Cytoplasmic FUS-containing aggregates are often associated with concomitant loss of nuclear FUS. Whether loss of nuclear FUS function, gain of a cytoplasmic function, or a combination of both lead to neurodegeneration remains elusive. To address this question, we generated knockin mice expressing mislocalized cytoplasmic FUS and complete FUS knockout mice. Both mouse models display similar perinatal lethality with respiratory insufficiency, reduced body weight and length, and largely similar alterations in gene expression and mRNA splicing patterns, indicating that mislocalized FUS results in loss of its normal function. However, FUS knockin mice, but not FUS knockout mice, display reduced motor neuron numbers at birth, associated with enhanced motor neuron apoptosis, which can be rescued by cell-specific CRE-mediated expression of wild-type FUS within motor neurons. Together, our findings indicate that cytoplasmic FUS mislocalization not only leads to nuclear loss of function, but also triggers motor neuron death through a toxic gain of function within motor neurons.

Keywords amyotrophic lateral sclerosis; frontotemporal dementia; FUS; motor neuron degeneration; PY-NLS

Subject Categories Molecular Biology of Disease; Neuroscience

DOI 10.15252/embj.201592559 | Received 26 July 2015 | Revised 28 January 2016 | Accepted 1 February 2016

Introduction

Mutations in several aggregation-prone RNA-binding proteins (RBPs) are increasingly linked to various neurodegenerative diseases. Such mutations constitute a major cause of amyotrophic lateral sclerosis (ALS), the most frequent adult-onset motor neuron disease, with mutations in TDP-43 (Gitcho *et al*, 2008; Kabashi *et al*, 2008; Sreedharan *et al*, 2008) and FUS (Kwiatkowski *et al*, 2009; Vance *et al*, 2009) accounting each for about 5% of familial ALS cases. Even in the absence of mutations, abnormal cytoplasmic inclusions of TDP-43 represent a pathological hallmark of sporadic ALS, non-SOD1 familial ALS, and frontotemporal dementia (FTD) (Neumann *et al*, 2006, 2009), a neurodegenerative condition characterized by behavioral and language deficits. Similarly, compromised FUS nuclear localization

1 Faculté de Médecine, INSERM U1118, Strasbourg, France
2 Université de Strasbourg UMR_S1118, Strasbourg, France
3 Molecular Neurogenetics Laboratory, Max Planck Institute for Molecular Biomedicine, Muenster, Germany
4 Faculty of Medicine, University of Muenster, Muenster, Germany
5 Department of Neurosciences, University of California, San Diego, La Jolla, CA, USA
6 Ludwig Institute for Cancer Research, University of California, San Diego, La Jolla, CA, USA
7 Institut Clinique de la souris, Illkirch-Graffenstaden, France
8 Department of Cellular and Molecular Medicine, University of California, San Diego, La Jolla, CA, USA
9 University of Cardiff, Cardiff, UK
10 Department of Neurology, University of Ulm, Ulm, Germany
11 Mammalian Cell Signaling Laboratory, Department of Vascular Cell Biology, Max Planck Institute for Molecular Biomedicine, Muenster, Germany
*Corresponding author. Tel: +49 251 8346895; E-mail: erik.storkebaum@mpi-muenster.mpg.de
**Corresponding author. Tel: +1 617 643 6774; E-mail: clagier-tourenne@mgh.harvard.edu
***Corresponding author. Tel: +33 3 68 85 30 82; E-mail: ldupuis@unistra.fr
†Present address: MassGeneral Institute for Neurodegenerative Disease, Department of Neurology, Massachusetts General Hospital, Harvard Medical School, Charlestown, MA, USA

and cytoplasmic FUS aggregates are found in ALS patients carrying *FUS* mutations, as well as in a subset of FTD patients without TDP-43 pathology (Mackenzie *et al*, 2010). Consistent with a central role of RNA processing misregulation in ALS and FTD pathogenesis, mutations in several other RBPs were recently identified, in particular TAF15 and EWSR1, two proteins from the same family as FUS (Couthouis *et al*, 2011, 2012), and other less closely related RBPs such as ataxin 2 (Elden *et al*, 2010), hnRNPA2B1 (Kim *et al*, 2013), hnRNPA1 (Kim *et al*, 2013), and matrin-3 (Johnson *et al*, 2014).

Disease-associated mutations in RBPs typically disrupt the normal nuclear localization of mutant proteins, with concomitant sequestration of the endogenous wild-type protein into cytoplasmic aggregates (Kim *et al*, 2013; Vance *et al*, 2013). Mutations are either located in highly unstructured prion-like protein domains, resulting in a higher propensity to aggregate (Kim *et al*, 2013), or in the vicinity of the nuclear localization signal (NLS), impairing nuclear import of the protein. For instance, the NLS of FUS is an atypical PY-NLS (Dormann *et al*, 2010) located at the C-terminus of the protein that represents a mutational hot spot in ALS patients. Along with missense mutations, several truncating or frameshift mutations deleting the FUS NLS have been identified in ALS patients (Fig EV1) and are often associated with juvenile onset and rapid disease progression (Baumer *et al*, 2010; Waibel *et al*, 2010, 2013; Zou *et al*, 2013; Calvo *et al*, 2014; Deng *et al*, 2014). In most instances, *FUS* mutations are dominantly inherited. However, it is noteworthy that a recessive inheritance pattern is occasionally observed in ALS patients (Kwiatkowski *et al*, 2009; Bertolin *et al*, 2014).

FUS and TDP-43 normally shuttle between the nucleus and cytoplasm, and defective nuclear import may lead to both loss of their nuclear functions and deregulation of their cytoplasmic roles. In the nucleus, FUS and TDP-43 are involved in regulation of pre-mRNA splicing, transcription, and microRNA biogenesis, all processes that may be affected by their depletion from the nucleus (Morlando *et al*, 2012; Ling *et al*, 2013). Consistently, reductions of TDP-43 or FUS were associated with altered expression and splicing of several hundreds of genes (Polymenidou *et al*, 2011; Tollervey *et al*, 2011; Ishigaki *et al*, 2012; Lagier-Tourenne *et al*, 2012; Rogelj *et al*, 2012; Ling *et al*, 2015), and both proteins are critically involved in the processing of long pre-mRNAs (Polymenidou *et al*, 2011; Lagier-Tourenne *et al*, 2012; Ling *et al*, 2013; Sibley *et al*, 2015). Cytosolic functions of FUS and TDP-43 include transport (Alami *et al*, 2014) and/or storage (Han *et al*, 2012) of mRNA in the cytoplasm with a crucial role in the formation of stress granules (Li *et al*, 2013).

Although several lines of evidence indicate that cytoplasmic mislocalization of RBPs is a key event in disease pathogenesis, definitive *in vivo* evidence is lacking and the relative contributions of loss and gain of function still need to be established. Indeed, it remains unknown whether loss of nuclear function of mutant RBPs is sufficient to trigger motor neuron disease or whether a cytosolic gain of function is also involved. There have been two major hurdles in answering these questions. First, ALS-associated RBPs are crucial for cell physiology, and overexpression of wild-type proteins causes widespread phenotypes (Huang *et al*, 2011; Mitchell *et al*, 2013; Sephton *et al*, 2014). This represents a major drawback when attempting to discern the pathophysiological effects of disease-causing mutations in overexpression models. Second, potent autoregulatory mechanisms control cellular levels of RBPs. For instance, both TDP-43 (Ayala *et al*, 2011; Polymenidou *et al*, 2011; D'Alton *et al*, 2015) and FUS (Lagier-Tourenne *et al*, 2012; Zhou *et al*, 2013; Dini Modigliani *et al*, 2014) control their own levels by binding to their mRNAs. As a consequence, the levels of endogenous TDP-43 or FUS proteins are strikingly reduced in animal models overexpressing wild-type or mutant TDP-43 and FUS (Wegorzewska *et al*, 2009; Huang *et al*, 2011; Arnold *et al*, 2013; Mitchell *et al*, 2013; Sephton *et al*, 2014).

Here, we use homologous recombination techniques to circumvent issues inherent to overexpression animal models. We systematically compare the pathological and molecular features of two novel mouse models either expressing a truncated FUS protein that lacks the NLS and localizes within the cytoplasm (knockin mice) or harboring a genomic mutation associated with complete absence of FUS protein (knockout mice). Both mice expressing mutant cytoplasmic FUS and mice completely devoid of FUS died at birth of respiratory insufficiency. Using genomic approaches, we determined that FUS knockin mice display expression and splicing alterations consistent with loss of FUS nuclear function. However, mice expressing truncated cytoplasmic FUS, but not FUS knockout mice, exhibit perinatal motor neuron loss, which can be rescued by motor neuron-restricted reversal of the mutant FUS gene to wild-type FUS. These findings demonstrate that cytoplasmic FUS leads to loss of nuclear FUS function, yet exerts a toxic gain of function within the cytoplasm of motor neurons necessary to trigger neuronal death.

Results

Cytoplasmic mislocalization of mutant FUS in *Fus*$^{\Delta NLS/\Delta NLS}$ mice

With the aim to investigate *in vivo* consequences of altered FUS localization, we generated a mouse model with targeted deletion of the PY-NLS, encoded by the last exon of the *Fus* gene (exon 15). This mutation closely mimics ALS-causing truncating mutations of *FUS* (Fig EV1). We opted for a strategy that would not only result in ablation of exon 15, but also allow for CRE-mediated reversal to the wild-type locus. Due to the small size of intron 14, we engineered the *Fus* locus to include, in intron 12, a floxed cDNA encoding exons 13 and 14 of *Fus*, followed by 3 transcription stop cassettes and a poly-adenylation signal (Fig 1A). Germ line transmission of the recombinant allele was obtained (Fig 1B) and mice heterozygous and homozygous for the targeted allele will hereafter be referred to as *Fus*$^{\Delta NLS/+}$ and *Fus*$^{\Delta NLS/\Delta NLS}$, respectively. Homozygous *Fus*$^{\Delta NLS/\Delta NLS}$ mice died shortly after birth, and tissues dissected at birth (P0) were analyzed for expression and localization of FUS$^{\Delta NLS}$ mRNA and protein. The ΔNLS mRNA could be detected by RT–PCR in tissues of *Fus*$^{\Delta NLS/+}$ and *Fus*$^{\Delta NLS/\Delta NLS}$ mice (Figs 1C and EV2A). FUS protein was detected by immunoblotting in *Fus*$^{\Delta NLS/+}$ and *Fus*$^{\Delta NLS/\Delta NLS}$ brain, spinal cord, and muscle protein extracts using antibodies targeting the internal or N-terminal parts of FUS (Figs 1D and EV2B). Contrastingly, no signal was found in *Fus*$^{\Delta NLS/\Delta NLS}$ protein extracts when using two different antibodies that recognize the C-terminal NLS of FUS (Figs 1D and EV2B), demonstrating that the engineered *Fus* gene leads to the generation of a FUS protein devoid of NLS. FUS protein levels were heterogeneous in *Fus*$^{\Delta NLS/+}$ brains (Fig 1D). As expected, FUS protein localized to the nucleus in cultured mouse embryonic fibroblasts

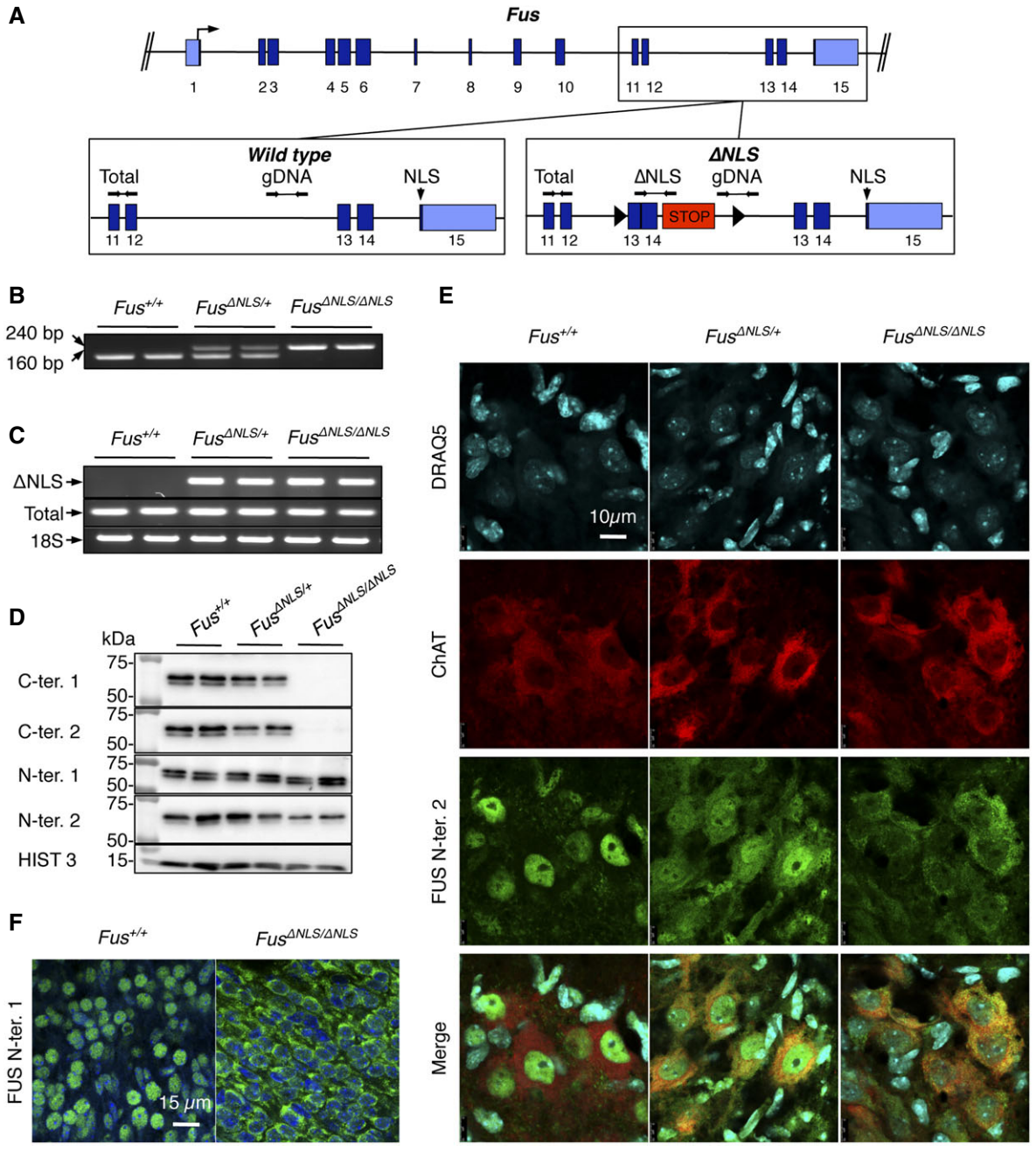

Figure 1. FUS mislocalization in *Fus$^{\Delta NLS/\Delta NLS}$* mice.

A Schematic representation of the *Fus* gene locus (upper panel). Lower panels depict exons 11–15 in the wild-type allele (left) and ΔNLS allele (right) with localization of PCR primers used for genotyping (gDNA, used in B) and for RT–PCR (Total and ΔNLS, used in C). Arrow: translational start site. STOP cassettes are indicated in red; loxP sites as black triangles; coding regions are in dark blue and UTRs in light blue. Location of the region encoding the nuclear localization signal (NLS) is indicated in exon 15.

B Representative PCR genotyping results from 2 *Fus$^{+/+}$*, 2 *Fus$^{\Delta NLS/+}$*, and 2 *Fus$^{\Delta NLS/\Delta NLS}$* knockin mice using primers designed around the distal loxP site of the *Fus$^{\Delta NLS}$* allele and shown as gDNA in (A). The expected size of the PCR product of the ΔNLS allele is 240 bp; the size of wild-type allele is 160 bp.

C RT–PCR analysis of brain from 2 *Fus$^{+/+}$*, 2 *Fus$^{\Delta NLS/+}$*, and 2 *Fus$^{\Delta NLS/\Delta NLS}$* knockin P0 mice using primers located in the STOP cassette, and thus specific to the ΔNLS mRNA (ΔNLS, upper panel), or primers located in exon 11, that is, upstream of the floxed cDNA insertion, and thus amplifying total *Fus*-derived mRNA (Total, middle panel). PCR amplification of 18S rRNA is shown as a standard gene (lower panel).

D Immunoblot analysis of FUS protein in cerebral cortex of 2 *Fus$^{+/+}$*, 2 *Fus$^{\Delta NLS/+}$*, and 2 *Fus$^{\Delta NLS/\Delta NLS}$* knockin mice using a combination of two different antibodies targeting either the C-terminal (C-ter. 1 and C-ter. 2) NLS, the N-terminal part (N-ter. 1), or an internal part (N-ter. 2) of FUS. Molecular weight markers are shown on the left, and apparent MW is indicated.

E Double immunostaining for the motor neuronal marker ChAT and Fus (N-terminal part) in the ventral horn of spinal cord.

F Double immunostaining for nuclei (DAPI, blue) and Fus (N-terminal part) in the cerebral cortex.

Source data are available online for this figure.

(MEFs) of $Fus^{+/+}$ mice. In striking contrast, FUS redistributed from the nuclear compartment to the cytoplasm in $Fus^{\Delta NLS/\Delta NLS}$ MEFs (Fig EV2C) and was detected in both the nucleus and the cytoplasm of $Fus^{\Delta NLS/+}$ MEFs (Fig EV2C). Consistently, in $Fus^{\Delta NLS/\Delta NLS}$ newborn mice, immunostaining revealed that mutant FUS is localized to the cytoplasm of spinal motor neurons and cortical neurons, contrasting with the normal nuclear localization in $Fus^{+/+}$ neurons (Fig 1E and F). In $Fus^{\Delta NLS/+}$ mice, FUS is detected in both the nucleus and the cytoplasm of motor neurons (Fig 1E). Thus, the $Fus^{\Delta NLS}$ allele effectively leads to the expression of a truncated FUS protein that lacks the NLS and localizes predominantly to the cytoplasm.

Both cytoplasmic mislocalization of FUS and complete loss of FUS result in perinatal lethality

$Fus^{\Delta NLS/\Delta NLS}$ mice were born alive, but died within minutes after birth, while $Fus^{\Delta NLS/+}$ mice survived the perinatal period. The body length and weight of $Fus^{\Delta NLS/\Delta NLS}$ pups were slightly but significantly reduced as compared to $Fus^{+/+}$ and $Fus^{\Delta NLS/+}$ newborn mice (Fig 2A–C). The cause of death appeared to be respiratory insufficiency, as $Fus^{\Delta NLS/\Delta NLS}$ animals showed poor respiratory movements and cyanosis, and H&E staining of sections through the lung revealed uninflated lungs with complete alveolar atelectasis (Fig 2D).

Cytoplasmic FUS mislocalization could have detrimental effects either through toxicity resulting from increased cytoplasmic FUS levels or through loss of its normal nuclear function. To distinguish between these possibilities, we investigated whether complete loss of FUS recapitulates the perinatal lethality phenotype of $Fus^{\Delta NLS/\Delta NLS}$ mice. Mice with a gene trap insertion in exons 8 or 12 of the *Fus* gene have been described previously (Hicks *et al*, 2000; Kuroda *et al*, 2000), yet both of these *Fus* gene trap lines express low amounts of truncated FUS protein, thus precluding their use to discriminate between loss- versus gain-of-function mechanisms. To tackle this issue, we generated a novel *Fus* knockout model (hereafter referred to as $Fus^{-/-}$) that was systematically compared to $Fus^{\Delta NLS/\Delta NLS}$ mice in the same C57Bl6 background. In this new *Fus* knockout allele, a trap cassette was inserted in intron 1 to completely disrupt transcription of the endogenous *Fus* gene (Fig 3A). Southern blot and direct sequencing confirmed the position and orientation of the gene trap insertion, and excluded additional insertion events elsewhere in the genome (not shown). FUS protein was undetectable in the central nervous system of $Fus^{-/-}$ newborn mice by Western blot using the above-described antibodies against the N-terminal and C-terminal parts of the protein (Fig 3B and C) and *Fus* mRNA could not be detected by quantitative real-time PCR (Fig 3D). Consistently, immunostaining for FUS on spinal cord sections of E18.5 $Fus^{-/-}$ mice did not detect FUS protein (Fig 3E), confirming that $Fus^{-/-}$ mice are FUS protein null. Depending on the genetic background, previously described *Fus* gene trap mice were reported either to be adult viable, to die before the age of weaning or within 16 h after birth (Hicks *et al*, 2000; Kuroda *et al*, 2000; Kino *et al*, 2015). In contrast, $Fus^{-/-}$ mice died within 30 min after birth due to respiratory insufficiency. Similar to $Fus^{\Delta NLS/\Delta NLS}$ pups, the body weight and body length of $Fus^{-/-}$ newborn mice were significantly reduced as compared to littermate controls (Fig 3F and G). Thus, both complete loss of FUS and its cytoplasmic mislocalization trigger a similar perinatal phenotype in C57Bl6 mice.

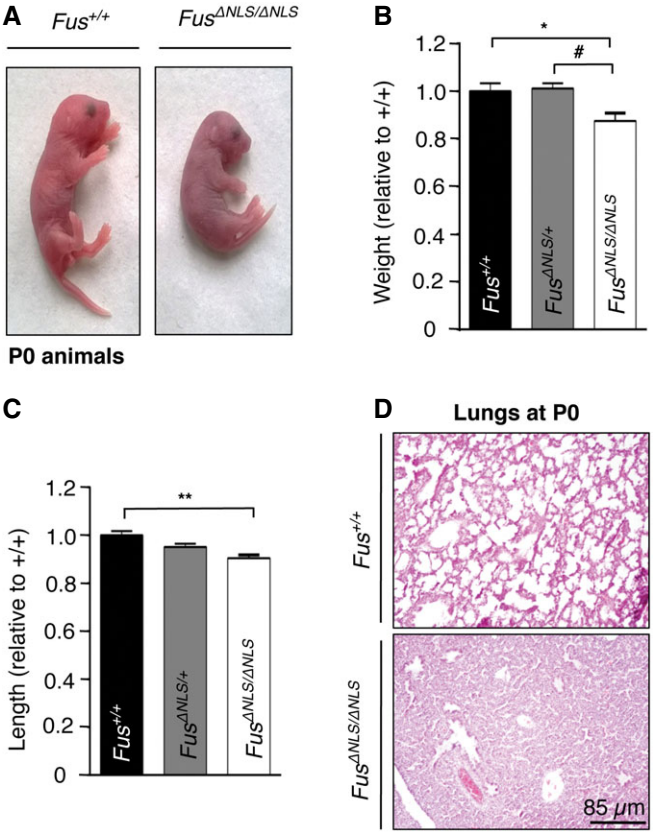

Figure 2. Perinatal lethality in $Fus^{\Delta NLS/\Delta NLS}$ mice.

A Photographs of $Fus^{+/+}$ and $Fus^{\Delta NLS/\Delta NLS}$ pups immediately after birth (P0 animals).

B, C $Fus^{\Delta NLS/\Delta NLS}$ mice showed significantly reduced body weight (B) and length (C). Weight and length values normalized to wild type ($Fus^{+/+}$) are presented (mean ± SEM). $N = 11$ $Fus^{+/+}$, $N = 26$ $Fus^{\Delta NLS/+}$ and $N = 14$ $Fus^{\Delta NLS/\Delta NLS}$; $^{*}P < 0.05$, $^{**}P < 0.01$ versus $Fus^{+/+}$, $^{\#}P < 0.05$ versus $Fus^{\Delta NLS/+}$; one-way ANOVA followed by Tukey's *post hoc* test.

D Representative hematoxylin and eosin stainings of lungs of $Fus^{+/+}$ and $Fus^{\Delta NLS/\Delta NLS}$ at birth.

Extensive overlap of RNA expression changes induced by cytoplasmic FUS mislocalization and complete loss of FUS

The phenotypic similarity of $Fus^{\Delta NLS/\Delta NLS}$ and $Fus^{-/-}$ newborn mice is consistent with FUS cytoplasmic mislocalization leading to loss of FUS nuclear function. FUS has been involved in the regulation of gene expression and alternative splicing of its mRNA targets (Polymenidou *et al*, 2011; Tollervey *et al*, 2011; Ishigaki *et al*, 2012; Lagier-Tourenne *et al*, 2012; Rogelj *et al*, 2012). In addition, FUS interacts with several proteins, including U1-snRNP (Yamazaki *et al*, 2012; Sun *et al*, 2015), SMN (Yamazaki *et al*, 2012; Groen *et al*, 2013; Tsuiji *et al*, 2013; Sun *et al*, 2015), HDAC1 (Wang *et al*, 2013), Drosha (Morlando *et al*, 2012), RNA polymerase II (Schwartz *et al*, 2012), and PRMT1 (Tibshirani *et al*, 2014), known to have profound effects on splicing and gene expression. Hence, the expression of a truncated cytoplasmic form of FUS may primarily lead to loss of nuclear FUS function and defective regulation of direct FUS RNA targets. In addition, cytoplasmic accumulation of FUS may also alter the function and/or

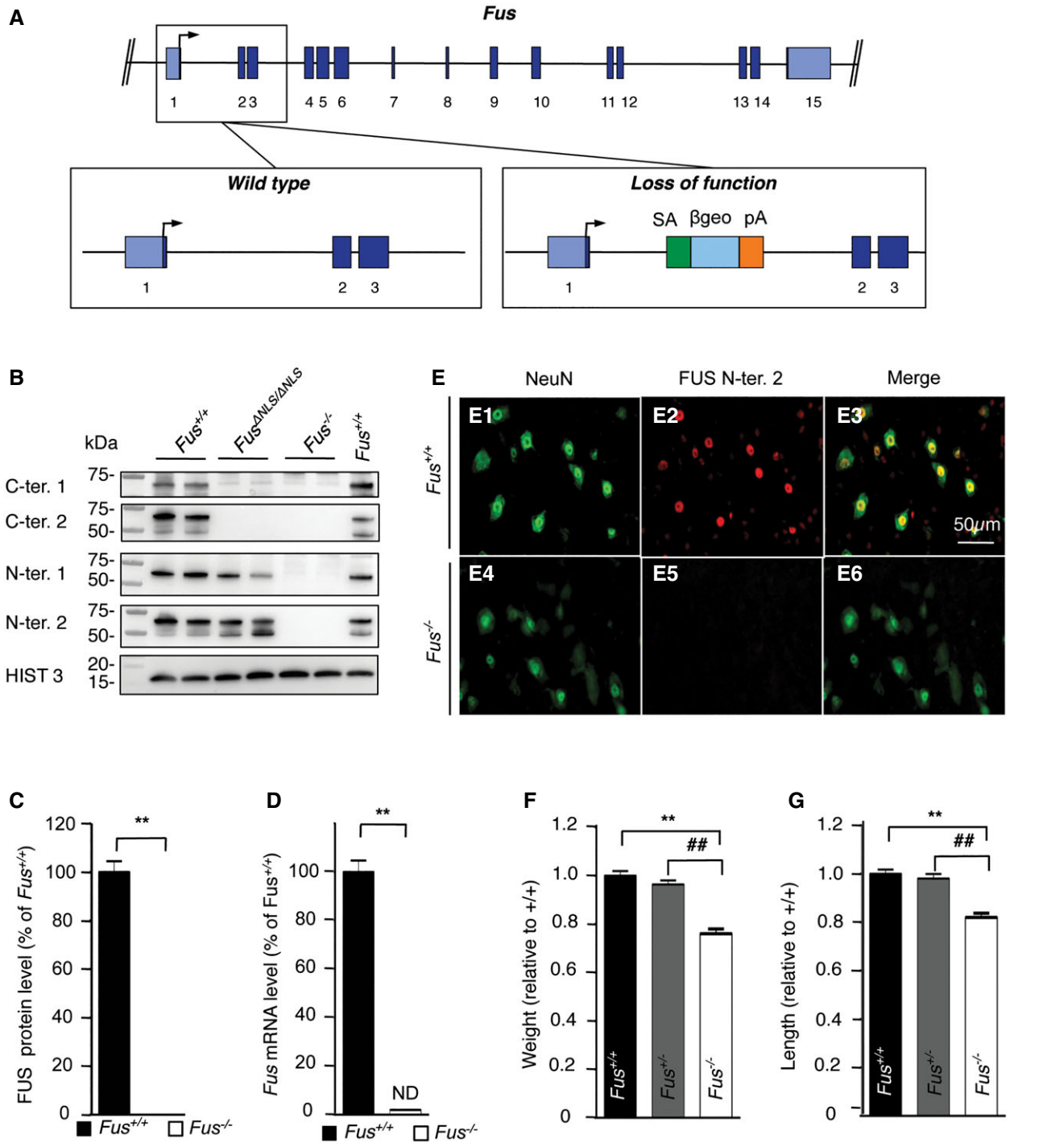

Figure 3. Generation of a complete *Fus*$^{-/-}$ loss-of-function mouse model.

A Schematic representation of the *Fus* gene locus (upper panel). Lower panels depict exons 1–3 in the wild-type allele (left) and loss-of-function allele (right). Arrow: translational start site; SA: splice acceptor; βgeo: β-galactosidase/neomycin phosphotransferase fusion gene; pA: polyA.

B Representative immunoblot for FUS on protein extracts of E18.5 brain. Histone 3 is used as a loading control.

C Quantification of FUS protein levels from immunoblots.

D Quantitative real-time PCR for *Fus* transcript in *Fus*$^{+/+}$ *and Fus*$^{-/-}$ mice. ND: not detected.

E Immunostaining for the neuronal marker NeuN and FUS on the spinal cord ventral horn of E18.5 *Fus*$^{+/+}$ and *Fus*$^{-/-}$ mice.

F, G Body weight (F) and length (G) of *Fus*$^{+/+}$, *Fus*$^{+/-}$, and *Fus*$^{-/-}$ pups at birth; $N = 14$ *Fus*$^{+/+}$, $N = 36$ *Fus*$^{+/-}$, and $N = 13$ *Fus*$^{-/-}$ for body weight; $N = 6$ per genotype for body length.

Data information: Data represent mean ± SEM. $^{**}P < 0.01$ versus *Fus*$^{+/+}$, $^{\#\#}P < 0.01$ versus *Fus*$^{+/-}$; one-way ANOVA followed by Tukey's *post hoc* test.
Source data are available online for this figure.

subcellular localization of FUS-interacting proteins and result in additional gene expression and splicing alterations. To discriminate between gain- and loss-of-function changes, we systematically compared RNA profiles in brains from $Fus^{\Delta NLS/\Delta NLS}$ and $Fus^{-/-}$ mice. First, we used strand-specific, genomewide sequencing of RNAs (Parkhomchuk *et al*, 2009) (RNA-seq) to evaluate RNA expression levels in brains of $Fus^{\Delta NLS/\Delta NLS}$ and $Fus^{-/-}$ mice. Total RNA was extracted from E18.5 embryonic brains of $Fus^{\Delta NLS/\Delta NLS}$ mice ($N = 5$), and wild-type littermates ($N = 4$), as well as homozygous $Fus^{-/-}$ ($N = 5$) and their control $Fus^{+/+}$ littermates ($N = 5$). Expression levels for each annotated protein-coding gene were determined by the number of mapped fragments per kilobase of exon, per million mapped reads (FPKM) (Mortazavi *et al*, 2008; Trapnell *et al*, 2012). The FPKM ratio of the *Fus* gene confirmed that *Fus* was expressed in $Fus^{\Delta NLS/\Delta NLS}$ mice, but not in $Fus^{-/-}$ mice (Fig EV3A). Inspection of the reads mapped on the *Fus* gene demonstrated the absence of reads throughout all exons for the $Fus^{-/-}$ mice, while only exon 15 was not integrated in *Fus* transcripts of $Fus^{\Delta NLS/\Delta NLS}$ mice (Fig 4A). *Fus* transcript levels as determined by FPKM ratio were not significantly different in $Fus^{\Delta NLS/\Delta NLS}$ and $Fus^{+/+}$ mice (Fig EV3A). Unsupervised hierarchical clustering with all genes reliably discriminated mutant genotypes from their controls (Fig EV3B and C), indicating that both *Fus* mutation and *Fus* deletion displayed RNA expression profiles divergent from wild type. Statistical comparison of FPKM values identified 237 genes upregulated and 549 genes downregulated in $Fus^{\Delta NLS/\Delta NLS}$ mice (Dataset EV1 and Fig 4B). Of note, only nine genes and 56 genes were upregulated and downregulated more than 1.5-fold, respectively (Dataset EV1). Identical analysis in $Fus^{-/-}$ mice identified 669 upregulated genes (29 genes more than 1.5-fold) and 889 downregulated genes (72 genes more than 1.5-fold) (Dataset EV2 and Fig 4C). Comparison of both models identified 353 genes that were altered in the same direction, consistent with loss of FUS nuclear function underlying the altered levels of these transcripts (Fig 4D and Dataset EV3).

Downregulation of selected genes in both mouse models was confirmed by qRT–PCR (Appendix Fig S1A) yielding data similar to the RNA-seq results (Fig 4E). Out of these, several genes have been previously involved in neurological diseases such as the *Abelson helper integration site 1* (*Ahi1*) gene mutated in the neurodevelopmental Joubert syndrome (Ferland *et al*, 2004), the *Dystrophia myotonica protein kinase* (*Dmpk*) gene implicated in myotonic dystrophy type 1, the *low* and *medium* molecular weight *neurofilament* subunits (*Nefl* and *Nefm*) (Bergeron *et al*, 1994), and the gene encoding tubulin alpha 4A (*Tuba4a*) that was recently implicated in ALS (Smith *et al*, 2014). Similarly, selected upregulated genes were confirmed by qRT–PCR (Fig 4E and Appendix Fig S1A), including *Taf15,* a FUS family member also mutant in ALS (Couthouis *et al*, 2011). Increased levels of *Taf15* in $Fus^{\Delta NLS/\Delta NLS}$ and $Fus^{-/-}$ mice are consistent with the presence of FUS binding sites on the *Taf15* transcript (Lagier-Tourenne *et al*, 2012) and may illustrate a mechanism of compensation induced by loss of FUS nuclear function. Overall, an extensive overlap in RNA expression changes was found in $Fus^{\Delta NLS/\Delta NLS}$ and $Fus^{-/-}$ brains consistent with loss of FUS nuclear function in knockin mice.

Cytoplasmic mislocalization of FUS leads to unique RNA expression changes

A subset of transcripts were altered uniquely in $Fus^{\Delta NLS/\Delta NLS}$ animals (Fig 4F and Appendix Fig S1B), including the *Vitronectin* (*Vtn*) gene, the *small nuclear ribonucleoprotein polypeptides B and B1* (*Snrpb*) gene, the *Trove2* gene encoding for the 60 kDa SS-A/Ro ribonucleoprotein, and the *U2AF homology motif kinase 1* (*Uhmk1*) gene encoding for the kinase interacting with stathmin (KIS) protein that was implicated in schizophrenia and the regulation of splicing (Manceau *et al*, 2008) and local translation in neuritic projections (Cambray *et al*, 2009; Pedraza *et al*, 2014). Interestingly, $Fus^{\Delta NLS/\Delta NLS}$ animals displayed increased mRNA levels of *Ephb3*, a member of Eph/ephrin signaling pathways crucial in synaptogenesis and previously involved in Alzheimer's disease (Sheffler-Collins & Dalva, 2012), while *EphA4,* another member of Eph/ephrin system, has been recently involved in ALS (Van Hoecke *et al*, 2012) (Fig 4F and Appendix Fig S1B). Thus, $Fus^{\Delta NLS/\Delta NLS}$ expression profiles largely recapitulated expression profiles of $Fus^{-/-}$ brains, yet a subset of genes was found specifically associated with the expression of cytoplasmic truncated FUS in $Fus^{\Delta NLS/\Delta NLS}$ brains.

Gene ontology analysis showed that transcripts whose expression was upregulated in $Fus^{\Delta NLS/\Delta NLS}$ animals were enriched for genes involved in mRNA translation and extracellular matrix constituents (Dataset EV4). In contrast, transcripts upregulated in $Fus^{-/-}$ brains revealed enrichment for nuclear and nucleolar proteins involved in the regulation of transcription, DNA replication, or regulation of RNA metabolic processes (Dataset EV5). Gene ontology

Figure 4. FUS-dependent expression changes in mouse brain.

A RNA-seq reads from brain of homozygous knockin ($Fus^{\Delta NLS/\Delta NLS}$, upper panel), homozygous knockout ($Fus^{-/-}$, middle panel), and control ($Fus^{+/+}$, lower panel) mice showing the absence of exon 15 (red arrow) in *Fus* mRNA in $Fus^{\Delta NLS/\Delta NLS}$ mice, while the entire *Fus* transcript is absent in $Fus^{-/-}$ mice (green arrows).

B Heat map with hierarchical clustering of RNA-seq data from biological replicates of $Fus^{\Delta NLS/\Delta NLS}$ ($N = 5$) and control littermates ($N = 4$), showing genes differentially regulated between both genotypes among which 237 are upregulated and 549 are downregulated in $Fus^{\Delta NLS/\Delta NLS}$ animals as defined by $P < 0.05$ adjusted for multiple testing.

C Heat map with hierarchical clustering of RNA-seq data from biological replicates of $Fus^{-/-}$ ($N = 5$) and control littermates ($N = 5$), showing genes differentially regulated between both genotypes, among which 669 are upregulated and 889 are downregulated in $Fus^{-/-}$ animals as defined by $P < 0.05$ adjusted for multiple testing.

D Venn diagram showing the number of overlapping genes misregulated in $Fus^{\Delta NLS/\Delta NLS}$ (blue circle) and $Fus^{-/-}$ (red circle) brains with 353 genes similarly downregulated or upregulated upon cytoplasmic mislocalization or complete loss of FUS.

E Normalized expression (based on FPKM from RNA-seq) of genes identified by RNA-seq to be significantly downregulated (*Ahi1, Kcnip1, Nefm, Nefl, Tuba4a, Dmpk, Rad9b, Stac3, Hist1h2bc, Hist1h1c*) or upregulated (*Fam193b, Pmm2, Bphl, Taf15*) in both $Fus^{\Delta NLS/\Delta NLS}$ and $Fus^{-/-}$ compared to their control. Error bars represent SEM in 4-5 biological replicates. $^{**}P < 0.01$, two-tailed student's *t*-test.

F Normalized expression (based on FPKM from RNA-seq) of genes identified by RNA-seq to be uniquely changed in $Fus^{\Delta NLS/\Delta NLS}$ mice (*Trove2, Uhmk1, Ssh3, Vtn, Snrpb, Ephb3*). Error bars represent SEM in 4–5 biological replicates. $^{*}P < 0.05$, $^{**}P < 0.01$, two-tailed Student's *t*-test.

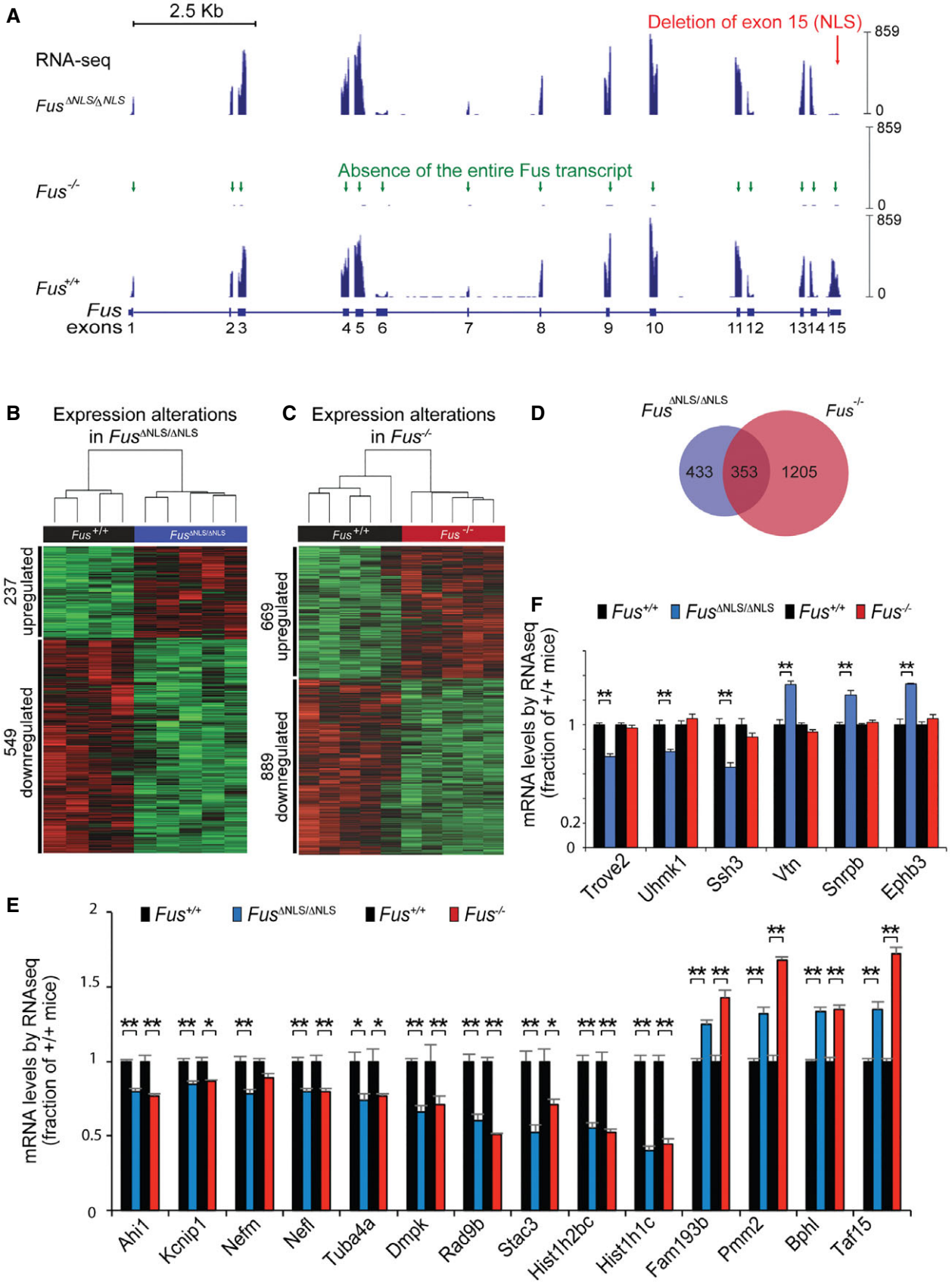
A
2.5 Kb
RNA-seq
Deletion of exon 15 (NLS)
Absence of the entire Fus transcript
Fus exons 1 2 3 4 5 6 7 8 9 10 11 12 13 14 15
B
Expression alterations in FusΔNLS/ΔNLS
237 upregulated
549 downregulated
C
Expression alterations in Fus-/-
669 upregulated
889 downregulated
D
433
353
1205
E
mRNA levels by RNAseq (fraction of +/+ mice)
Ahi1
Kcnip1
Nefm
Nefl
Tuba4a
Dmpk
Rad9b
Stac3
Hist1h2bc
Hist1h1c
Fam193b
Pmm2
Bphl
Taf15
F
mRNA levels by RNAseq (fraction of +/+ mice)
Trove2
Uhmk1
Ssh3
Vtn
Snrpb
Ephb3

Figure 4.

analysis revealed a similar enrichment for synaptic activity and function among transcripts downregulated in $Fus^{\Delta NLS/\Delta NLS}$ and $Fus^{-/-}$ animals (Datasets EV4 and EV5), supporting that cytoplasmic mislocalization of FUS alters the expression of genes involved in synaptogenesis, as a direct consequence of FUS loss of function. Contrastingly, gain of function elicited by cytoplasmic FUS might be more related to alterations in genes related to mRNA translation and extracellular matrix.

Widespread splicing alterations induced by cytoplasmic mislocalization and loss of FUS

To further compare the molecular changes elicited by cytoplasmic FUS mislocalization and FUS loss of function, we asked whether regulation of mRNA splicing was similarly affected in E18.5 brains of $Fus^{\Delta NLS/\Delta NLS}$ mice and $Fus^{-/-}$ mice. To characterize mRNA splicing, we exploited the RNA-mediated oligonucleotide annealing, selection, and ligation with next-generation sequencing (RASL-seq) method (Li *et al*, 2012; Zhou *et al*, 2012). This approach allowed us to quantitatively profile 3,859 unique alternative splicing events that correspond to exon inclusion or skipping events conserved between mouse and human (Fig EV4). Ratios of shorter to longer mRNA isoform counts were calculated and used to statistically compare the splicing changes between different groups. Unsupervised hierarchical clustering for all splicing events showed that mutant and deleted *Fus* mice clustered apart from their controls (Fig EV4B and C). In $Fus^{\Delta NLS/\Delta NLS}$ brains, 9.3% (173 events) of the 1,852 detected splicing events were different from controls, with 101 increased long splicing isoforms and 72 enhanced short isoforms (defined by *t*-test with $P < 0.05$ and average fold change > 1.5) (Fig 5A and Dataset EV6). Heterozygous $Fus^{\Delta NLS/+}$ mice clustered with wild-type mice demonstrating that their splicing profile is not significantly altered (Appendix Fig S2). Nevertheless, heat map of the 173 events significantly changed in homozygous $Fus^{\Delta NLS/\Delta NLS}$ mice showed an intermediate pattern in $Fus^{\Delta NLS/+}$ heterozygous littermates supporting a partial loss of FUS function in these mice (Appendix Fig S2). In $Fus^{-/-}$ brains, 17.9% (252 events) of the 1,406 detected splicing events were different from control littermates, with 118 increased long isoforms and 134 enhanced short isoforms (Fig 5B and Dataset EV7).

Comparison of the splicing changes between $Fus^{\Delta NLS/\Delta NLS}$ and $Fus^{-/-}$ mice revealed a striking overlap between both models. Seventy-five splicing events were commonly regulated in $Fus^{\Delta NLS/\Delta NLS}$ and $Fus^{-/-}$ mice, 100% of which were differentially included or excluded in the same direction (Fig EV4D and E and Dataset EV8).

Semi-quantitative RT–PCR of selected RNAs confirmed these FUS-dependent splicing changes (Figs 5C and EV4F), including transcripts previously implicated in neurodegenerative diseases such as the N-myc downstream-regulated gene 2 (*Ndrg2*) that is misaccumulated in Alzheimer's disease (Mitchelmore *et al*, 2004), the microtubule-associated protein tau (*Mapt*) gene mutated in frontotemporal dementia (Hutton *et al*, 1998), the ataxin 2 (*Atxn2*) gene mutated in ALS (Elden *et al*, 2010), spinocerebellar ataxia type 2 (SCA2) (Imbert *et al*, 1996), and the pro-neurotrophin receptor sortilin 1 (*Sort1*) (Hu *et al*, 2010). Interestingly, inclusion of sortilin 1 exon 17b [also referred to as exon 18 in Polymenidou *et al* (2011)] was previously associated with low levels of TDP-43 (Polymenidou *et al*, 2011; Prudencio *et al*, 2012) and found significantly increased in cortex of FTD patients with TDP-43 proteinopathy (Prudencio *et al*, 2012). Here, we observe that *Fus* mutation and deletion have an opposite effect on sortilin 1 as compared to TDP-43, with decreased inclusion of exon 17b in embryonic brains from both $Fus^{\Delta NLS/\Delta NLS}$ and $Fus^{-/-}$ mice (Figs 5C and EV4F).

Despite expected developmental differences in the alternative splicing patterns of embryonic and adult brains, 57 splicing events found misregulated by RASL-seq in $Fus^{\Delta NLS/\Delta NLS}$ and $Fus^{-/-}$ mice were also identified by Affymetrix microarrays in striatum from adult wild-type mice with antisense oligonucleotide-mediated depletion of *Fus* (Lagier-Tourenne *et al*, 2012), or in embryonic brains from another *Fus* knockout model that expresses low levels of truncated FUS protein (Hicks *et al*, 2000; Lagier-Tourenne *et al*, 2012). Among FUS-dependent alterations, abnormal splicing of *Mapt* exon 10 (Figs 5C and EV4F) is of particular relevance for disease pathogenesis as mutations enhancing exon 10 inclusion are linked to frontotemporal dementia (Liu & Gong, 2008). While in embryonic mouse brains the predominant mRNA isoforms of *Mapt* do not include exon 10 and encode for tau protein with three microtubule binding repeats (3R-tau) (McMillan *et al*, 2008; Dillman *et al*, 2013), we observed increased inclusion of exon 10 encoding for the 4-repeat tau isoform (4R tau) in both $Fus^{\Delta NLS/\Delta NLS}$ and $Fus^{-/-}$ mice. In all, splicing alterations caused by cytoplasmic FUS mislocalization are largely overlapping with those elicited by complete loss of FUS. Nevertheless, a subset of events were uniquely found in $Fus^{\Delta NLS/\Delta NLS}$ (Fig EV4D), which may be the consequence of functional disruption of other RNA-binding proteins by abnormal accumulation of FUS in the cytoplasm.

Cytoplasmic mislocalization of FUS leads to increased perinatal motor neuron apoptosis

We next asked whether perinatal death of $Fus^{\Delta NLS/\Delta NLS}$ and $Fus^{-/-}$ mice was accompanied by loss of motor neurons in the lumbar spinal cord. Immunostaining for choline acetyltransferase (ChAT), which specifically labels large motor neurons in the spinal cord ventral horn, revealed that the number of motor neurons was reduced by approximately 30% in $Fus^{\Delta NLS/\Delta NLS}$ mice as compared with both $Fus^{+/+}$ and $Fus^{\Delta NLS/+}$ mice (Fig 6A and B). To exclude

Figure 5. FUS-dependent alternative splicing alterations in mouse brain.

A Heat map with hierarchical clustering of RASL-seq data from biological replicates of $Fus^{\Delta NLS/\Delta NLS}$ ($N = 4$) and control littermates ($N = 4$), showing 173 alternative splicing alterations associated with expression of cytoplasmic FUS in knockin animals.

B Heat map with hierarchical clustering of RASL-seq data from biological replicates of $Fus^{-/-}$ ($N = 5$) and control littermates ($N = 5$), showing 252 alternative splicing alterations associated with loss of FUS in knockout animals.

C Semi-quantitative RT–PCR analyses of selected targets. Left panels show representative acrylamide gel pictures of RT–PCR products. Quantification of splicing changes from at least three biological replicates of $Fus^{\Delta NLS/\Delta NLS}$ (blue bars) and $Fus^{-/-}$ (red bars) compared to their control littermates ($Fus^{+/+}$, black bars) by semi-quantitative RT–PCR (middle panel) and RASL-seq (right panel) are shown. Error bars represent SEM. $^{*}P < 0.05$, $^{**}P < 0.01$, two-tailed Student's *t*-test.

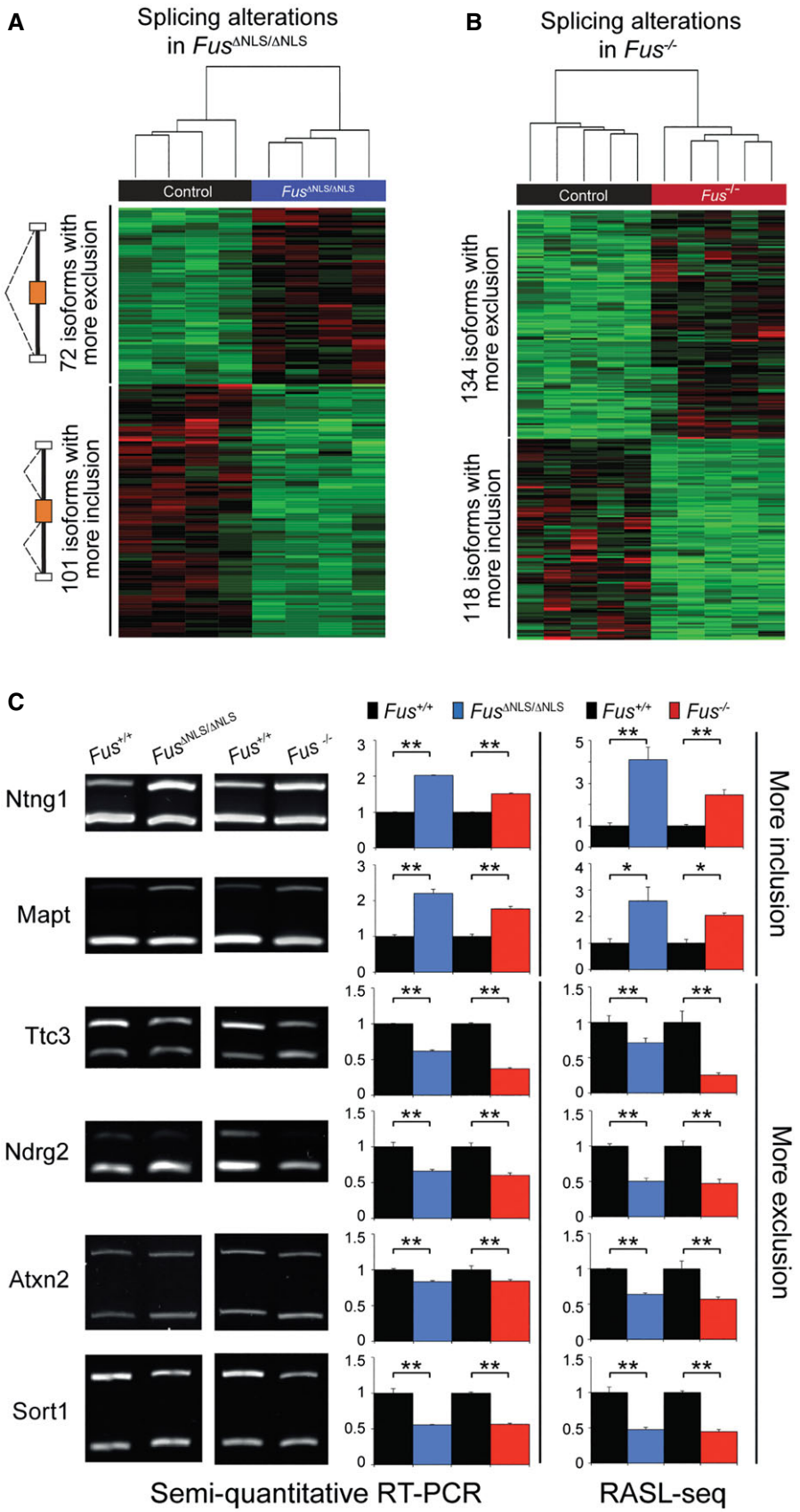

Figure 5.

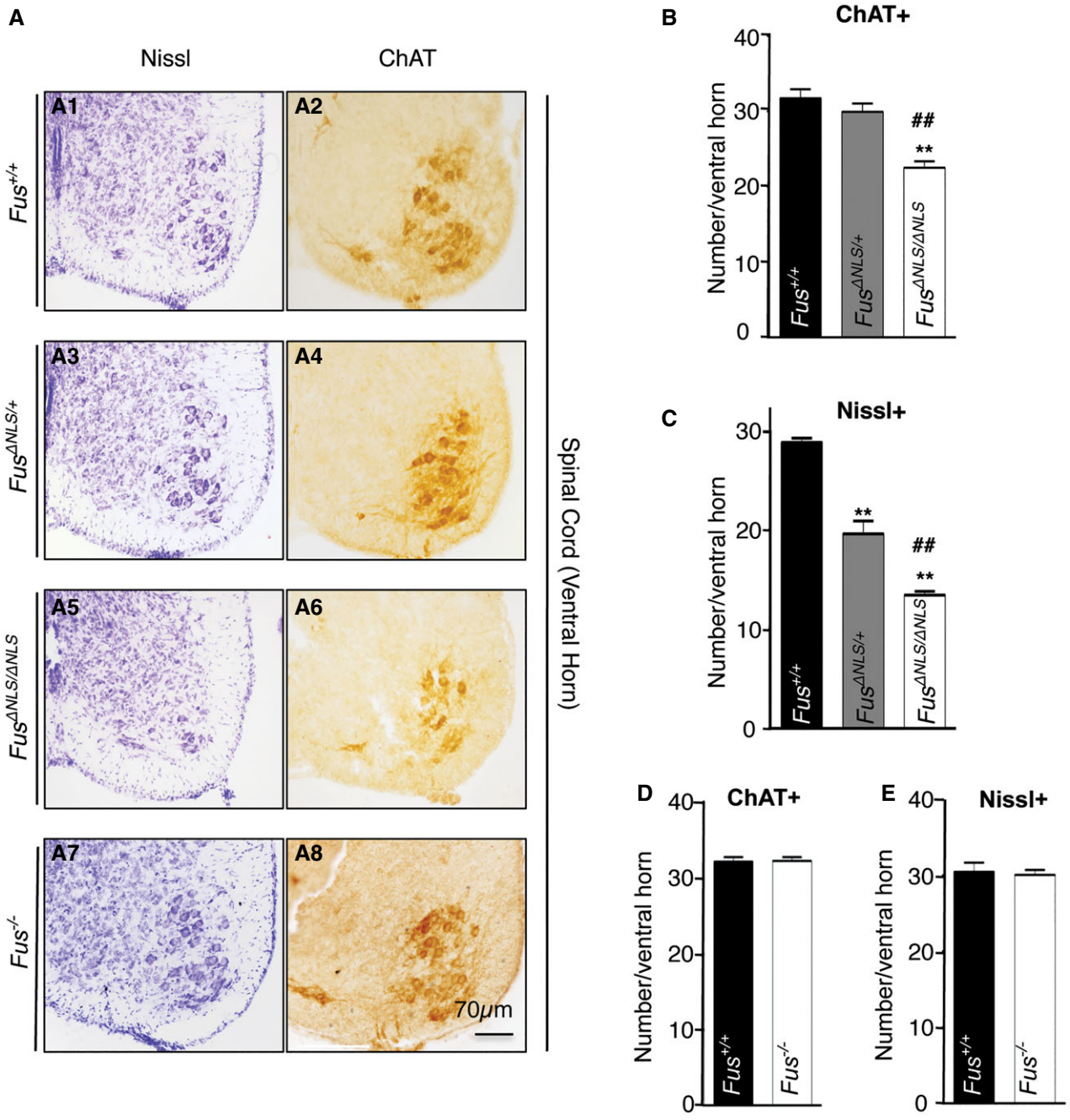

Figure 6. Motor neuron loss in $Fus^{\Delta NLS/\Delta NLS}$ mice.

A Representative light microscopy images of spinal cord sections of $Fus^{+/+}$, $Fus^{\Delta NLS/+}$, $Fus^{\Delta NLS/\Delta NLS}$, and $Fus^{-/-}$ mice at birth stained with cresyl violet (Nissl, A^1, A^3 A^5, A^7), or anti-choline acetyltransferase (ChAT, A^2, A^4 A^6, A^8).

B, C Quantification of $ChAT^+$ motor neurons (B) and $Nissl^+$ motor neurons (defined as Nissl-positive cells with a soma area > 80 μm^2) (C) per spinal cord ventral horn in $Fus^{\Delta NLS/\Delta NLS}$ mice (mean ± SEM). For $Nissl^+$ $N = 8$ $Fus^{+/+}$, $N = 5$ $Fus^{\Delta NLS/+}$, $N = 7$ $Fus^{\Delta NLS/\Delta NLS}$, and for $ChAT^+$ $N = 7$ per genotype, $^{**}P < 0.01$ versus $Fus^{+/+}$, $^{\#\#}P < 0.01$ versus $Fus^{\Delta NLS/+}$; one-way ANOVA followed by Tukey's *post hoc* test.

D–E Quantification of $ChAT^+$ (D) and $Nissl^+$ (E) motor neurons per spinal cord ventral horn in $Fus^{-/-}$ mice (mean ± SEM). $N = 6$ per genotype, no significant differences were found, by Student's unpaired *t*-test.

the possibility that this reduced number of ChAT-positive motor neurons reflected downregulation of ChAT expression rather than loss of motor neurons, we also performed Nissl staining, a histochemical stain that does not rely on the expression level of a specific marker. Quantification of neurons with an area of ≥ 80 μm^2 revealed a 50% reduction in the number of large motor neurons in the ventral horn of $Fus^{\Delta NLS/\Delta NLS}$ newborn mice (Fig 6C). Interestingly, $Fus^{\Delta NLS/+}$ mice displayed a smaller but statistically significant

loss of large Nissl-stained cells, suggesting that motor neurons were also affected in these mice despite showing normal numbers of ChAT-positive cells. In striking contrast with the situation in $Fus^{\Delta NLS/\Delta NLS}$ mice, spinal motor neuron counts were similar between $Fus^{-/-}$ mice and their wild-type littermates (Fig 6A, D and E), demonstrating that the mutant FUS protein expressed in $Fus^{\Delta NLS/\Delta NLS}$ mice is toxic to motor neurons during development. Besides motor neuron degeneration, neither $Fus^{\Delta NLS/\Delta NLS}$ nor $Fus^{-/-}$ mice displayed gross developmental abnormalities of the brain. Indeed, cortical thickness appeared normal in both mouse strains (Appendix Fig S3). In addition, the thickness of layers II-IV and layers V-VI defined by CUX1 and CTIP2 immunofluorescence, respectively, was normal in both mouse strains (Appendix Fig S4).

At birth, mouse motor neurons are still in the developmental period, and motor neurons that did not efficiently create synaptic contacts with muscles undergo apoptosis until P10 (Kanning *et al*, 2010). Supporting an increased perinatal motor neuron apoptosis in $Fus^{\Delta NLS/\Delta NLS}$ mice, the number of apoptotic cells detected by terminal deoxynucleotidyl transferase dUTP nick end labeling (TUNEL) was threefold higher in lumbar spinal cord sections of $Fus^{\Delta NLS/\Delta NLS}$ newborn mice than in wild-type littermates (Fig 7A and B). Furthermore, double immunostaining for ChAT and active caspase-3, labeling motor neurons actively undergoing apoptosis, revealed that motor neuron apoptosis was three times more frequent in $Fus^{\Delta NLS/\Delta NLS}$ than in wild-type littermates (Fig 7C–E). Together, these data indicate that cytoplasmic mislocalization of FUS leads to increased motor neuron death resulting in reduced numbers of lower motor neurons. The absence of motor neuron loss in $Fus^{-/-}$ mice indicates that cytoplasmic FUS accumulation leads to motor neuron death through a toxic gain-of-function mechanism.

Cytoplasmic mislocalization of FUS alters SMN and HDAC1 localization and induces eIF2α phosphorylation

We then asked whether cytoplasmic mislocalization of FUS in $Fus^{\Delta NLS/\Delta NLS}$ mice would affect the subcellular localization of some of its interaction partners. Immunostaining for SMN1 revealed that SMN1-positive nuclear gems were lost in motor neurons of $Fus^{\Delta NLS/\Delta NLS}$ mice (Fig 8A), as in cells from ALS patients and mouse models (Yamazaki *et al*, 2012; Tsuiji *et al*, 2013; Sun *et al*, 2015; Yu *et al*, 2015) and consistent with enhanced interaction between mutant FUS and SMN1 (Yamazaki *et al*, 2012; Gerbino *et al*, 2013; Groen *et al*, 2013; Sun *et al*, 2015; Yu *et al*, 2015). Furthermore, HDAC1, another FUS interaction partner (Wang *et al*, 2013), showed profoundly abnormal immunoreactivity in $Fus^{\Delta NLS/\Delta NLS}$ mice. Indeed, HDAC1 was diffusely nuclear in cells from wild-type spinal cords, while in $Fus^{\Delta NLS/\Delta NLS}$ animals HDAC1 immunoreactivity was condensed in 1–3 nuclear foci per cell (Fig 8B). Double immunofluorescence in spinal cords from control animals found a weak HDAC1 staining in ChAT-positive motor neurons contrasting with a strong nuclear signal in neighboring cells. The pattern was strikingly different in $Fus^{\Delta NLS/\Delta NLS}$ animals with HDAC1 aggregation into nuclear foci in ChAT-positive motor neurons (Fig 8C). In contrast to SMN1 and HDAC1, the binding partner of FUS TAF15 remained mostly nuclear in motor neurons from $Fus^{\Delta NLS/\Delta NLS}$ mice (Appendix Fig S5). Thus, cytoplasmic mislocalization of FUS perturbs the localization, and potentially the function, of specific interaction partners in motor neurons.

In autopsy material of ALS-FUS patients, FUS-containing cytoplasmic aggregates are found in neurons and glial cells. These aggregates are usually also immunopositive for ubiquitin (Vance *et al*, 2009; Baumer *et al*, 2010; Huang *et al*, 2010; Kobayashi *et al*, 2010; Tateishi *et al*, 2010). Despite motor neuron loss in $Fus^{\Delta NLS/\Delta NLS}$ mice, we did not observe FUS-positive (Fig 1E and F) aggregates in motor neurons or cortical neurons of newborn $Fus^{\Delta NLS/\Delta NLS}$ mice. We also did not observe ubiquitin-positive, poly-ubiquitin-positive, or neurofilament-positive aggregates in the ventral spinal cord of $Fus^{\Delta NLS/\Delta NLS}$ mice (Fig EV5A and B). As FUS is recruited to stress granules, and since neuropathology revealed that cytoplasmic protein aggregates in ALS-FUS patients stain positive for stress granule markers (Baumer *et al*, 2010; Dormann *et al*, 2010; Liu-Yesucevitz *et al*, 2010), we evaluated the distribution of TIAR, a stress granule marker in the spinal cord ventral horn in $Fus^{\Delta NLS/\Delta NLS}$ mice. TIAR displayed a similar diffuse cytosolic pattern in motor neurons of $Fus^{\Delta NLS/\Delta NLS}$ and control mice (Fig EV5C). As an additional marker for cellular stress, we evaluated eIF2α phosphorylation, which occurs in response to cellular stress and results in decreased global protein translation (Holcik & Sonenberg, 2005; Sonenberg & Hinnebusch, 2009). Immunostaining for the phosphorylated form of eIF2α revealed a diffuse cytoplasmic staining that was substantially more intense in spinal motor neurons of $Fus^{\Delta NLS/\Delta NLS}$ mice as compared to controls (Fig 8D) reflecting cellular stress in $Fus^{\Delta NLS/\Delta NLS}$ motor neurons, with consequent repression of protein translation.

Taken together, cytoplasmic mislocalization of FUS in motor neurons led to altered subcellular localization of several of its binding partners accompanied by stress-induced translational repression, but without the induction of protein aggregation or stress granule formation.

Cytoplasmic FUS mislocalization is intrinsically toxic to motor neurons

We subsequently asked whether FUS mislocalization within motor neurons is necessary to induce motor neuron loss in $Fus^{\Delta NLS/\Delta NLS}$ mice and therefore evaluated whether restricted expression of wild-type FUS in motor neurons could rescue their survival despite accumulation of the mutant protein in neighboring cells. We exploited the presence of loxP sites flanking the STOP cassette (Fig 1A) to selectively revert the ΔNLS allele to wild type in motor neurons. For this purpose, $Fus^{\Delta NLS/+}$ mice were crossed to mice expressing the CRE recombinase from the *ChAT* locus, which leads to CRE recombinase activity in virtually all cholinergic neurons (Rossi *et al*, 2011; Saxena *et al*, 2013). We expected that $Fus^{\Delta NLS/\Delta NLS}$/ChAT-CRE mice would express truncated FUS protein ubiquitously, except for cholinergic neurons. Double immunostaining for FUS and ChAT on spinal cord sections of $Fus^{\Delta NLS/\Delta NLS}$/*ChAT*-CRE newborn mice revealed that FUS nuclear localization was indeed largely restored in cholinergic neurons in the ventral spinal cord, but not in other neighboring cells, consistent with motor neuron selective CRE expression (Fig 9A). The rescue of FUS nuclear localization was either complete or only partial, with in the latter case motor neurons showing mixed cytoplasmic/nuclear FUS localization (Fig 9A), consistent with CRE having successfully recombined at least one $Fus^{\Delta NLS}$ allele to wild type. Neonatal lethality of $Fus^{\Delta NLS/\Delta NLS}$ mice was not rescued by the

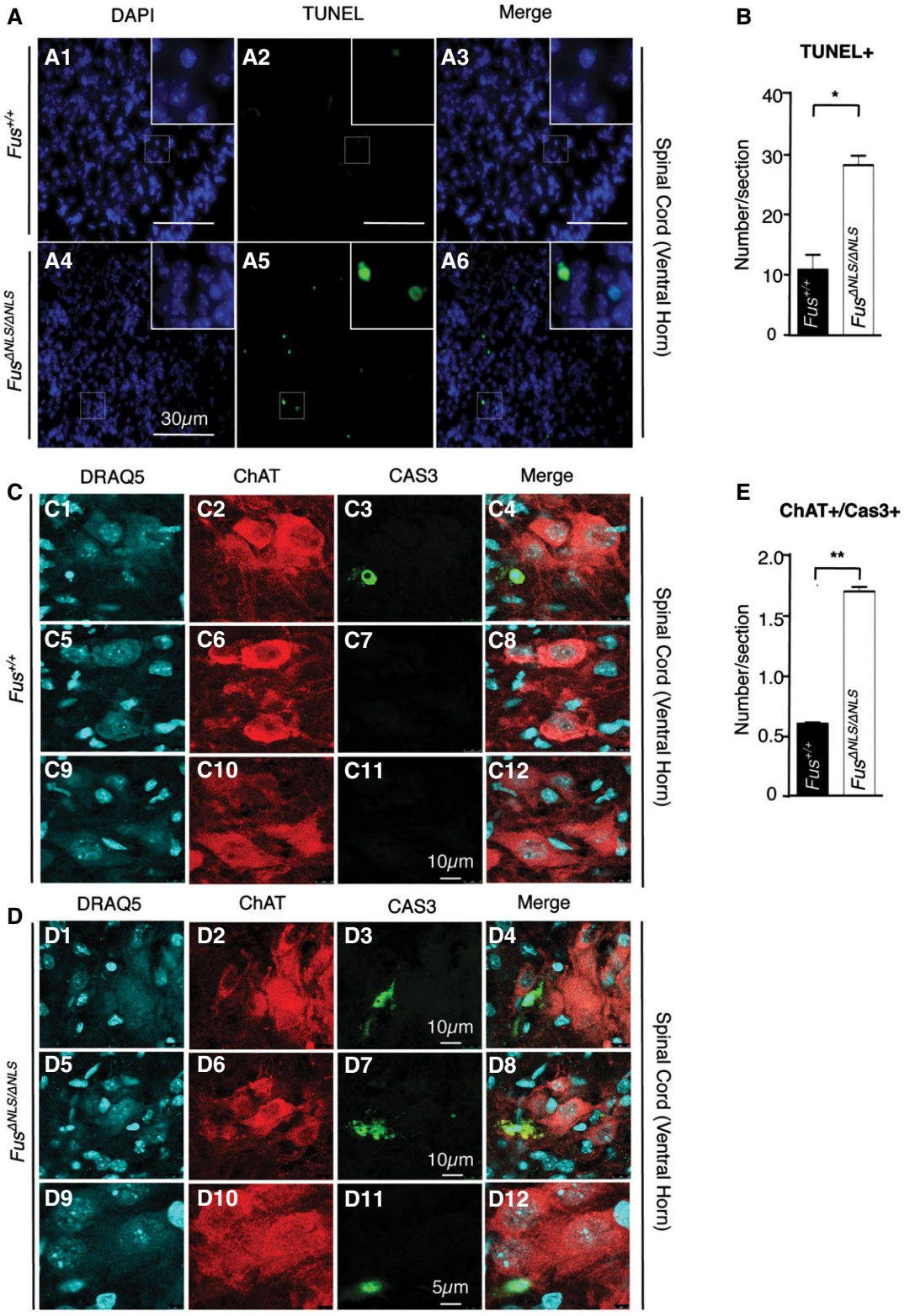

Figure 7. Motor neuron apoptosis in *Fus*$^{\Delta NLS/\Delta NLS}$ mice.

A Representative images of TUNEL assay in spinal cord of *Fus*$^{\Delta NLS/\Delta NLS}$ mice (A^4-A^6) and *Fus*$^{+/+}$ mice (A^1-A^3).

B Quantification of the total number of TUNEL and DRAQ5 (blue) double-positive cells in *Fus*$^{\Delta NLS/\Delta NLS}$ and *Fus*$^{+/+}$ per spinal cord section. Mean ± SEM, $N = 3$ per genotype, $^*P < 0.05$, by Student's unpaired *t*-test.

C, D Immunofluorescence microscopy of spinal cord of *Fus*$^{+/+}$ (C) and *Fus*$^{\Delta NLS/\Delta NLS}$ (D) mice showing active caspase-3 (green), ChAT (red), and DNA (cyan, DRAQ5).

E Quantification of caspase-3 (Cas3)/ChAT/DRAQ5 triple-positive cells in *Fus*$^{\Delta NLS/\Delta NLS}$ mice. Mean ± SEM, $N = 7$ per genotype, $^{**}P < 0.01$, by Student's unpaired *t*-test.

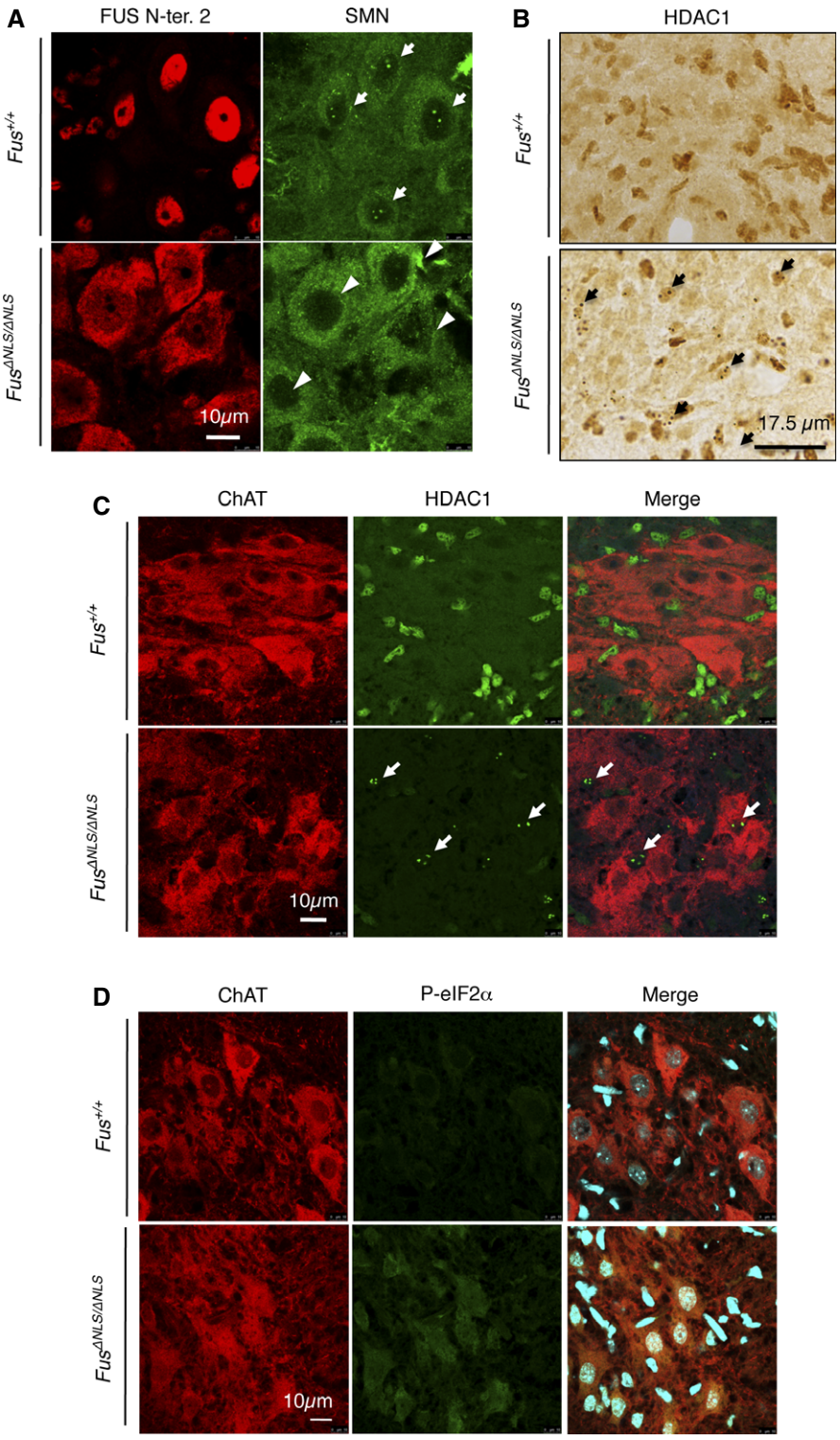

Figure 8. Alterations of SMN, HDAC1, and eIF2α in *Fus*$^{\Delta NLS/\Delta NLS}$ mice.

A Representative images of SMN (green) immunofluorescence in spinal cord. Nuclear gems, corresponding to SMN-immunoreactive foci in nuclei, are marked by arrows.

B HDAC1 immunoreactivity in spinal cord sections of *Fus*$^{+/+}$ and *Fus*$^{\Delta NLS/\Delta NLS}$ mice. Arrows point to HDAC1-immunoreactive nuclear foci.

C Representative images of immunofluorescence staining of motor neurons, labeled with ChAT (red) and HDAC1 (green). Examples of HDAC1 immunoreactive foci in motor neurons are indicated by arrows.

D Representative images of immunofluorescence staining of motor neurons labeled with ChAT (red) and phosphorylated eIF2α (green), a general translational stress response marker. DRAQ5 (cyan) was used to label nuclei.

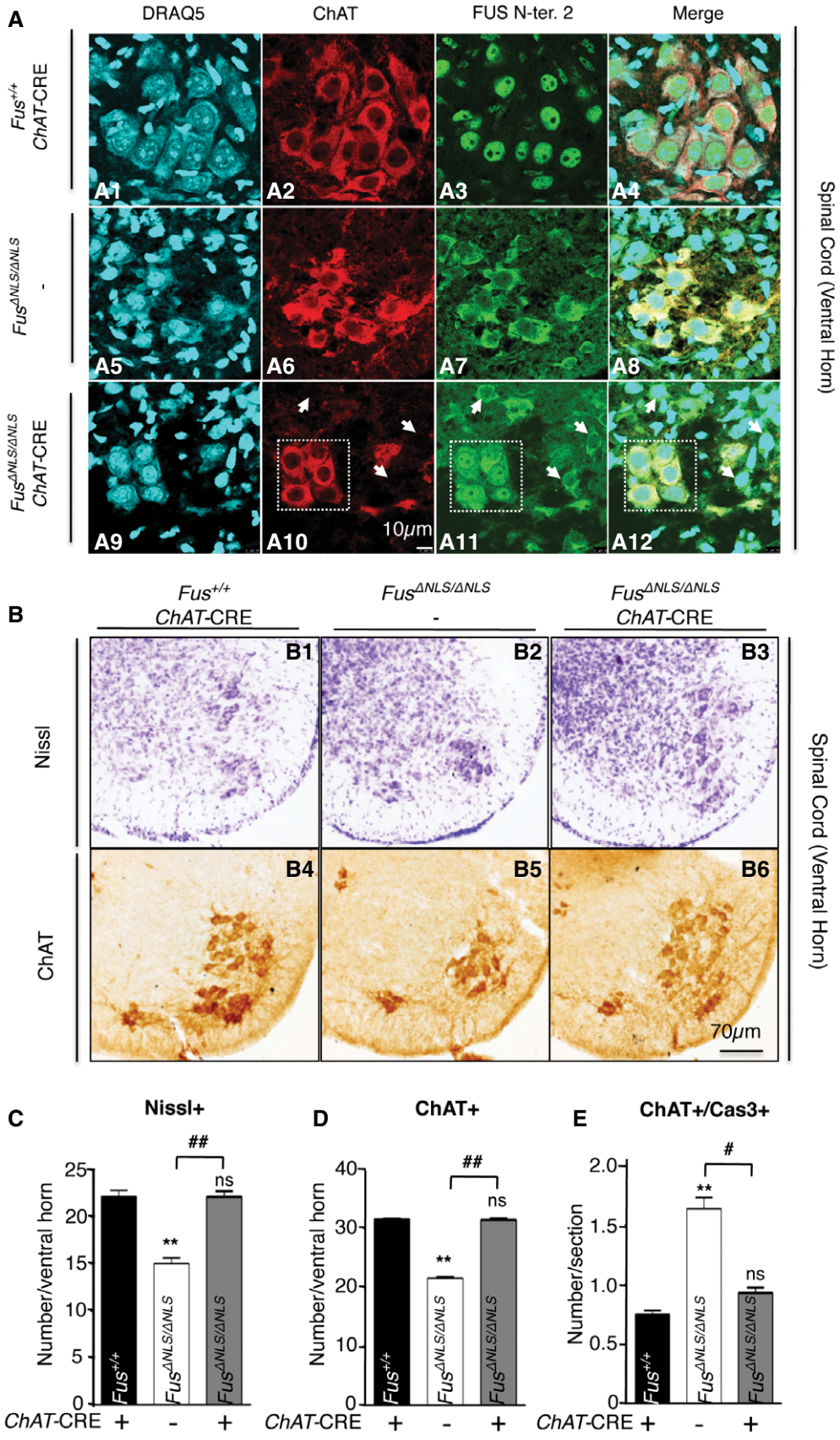

Figure 9.

Figure 9. Selective restoration of FUS nuclear import in motor neurons rescues motor neuron loss.

A Double immunolabeling of spinal cord neurons with ChAT (red) and N-terminal FUS antibody (green). Nuclei were visualized with DRAQ5 (blue). Cellular localization of FUS was analyzed in the ventral spinal cord of $Fus^{+/+}$/*ChAT*-CRE (A^1-A^4), $Fus^{\Delta NLS/\Delta NLS}$/− ($A^5$-$A^8$), and $Fus^{\Delta NLS/\Delta NLS}$/*ChAT*-CRE ($A^9$-$A^{12}$). FUS was completely nuclear in ChAT$^+$ neurons of $Fus^{+/+}$/*ChAT*-CRE, while cytoplasmic in $Fus^{\Delta NLS/\Delta NLS}$/−. In the ventral horn of $Fus^{\Delta NLS/\Delta NLS}$/*ChAT*-CRE mice, ChAT$^+$ neurons (motor neurons, e.g., within the dashed square) displayed nuclear FUS immunoreactivity, while ChAT-negative cells retained cytoplasmic FUS immunoreactivity (arrows).

B Representative light microscopy images of spinal cord sections of $Fus^{+/+}$/*ChAT*-CRE (B^1, B^4), $Fus^{\Delta NLS/\Delta NLS}$/− ($B^2$, B^5), and $Fus^{\Delta NLS/\Delta NLS}$/*ChAT*-CRE ($B^3$, B^6) mice at birth stained with cresyl violet (Nissl, B^1-B^3) or anti-choline acetyltransferase (ChAT, B^4-B^6).

C, D Quantification of Nissl$^+$ (C) and ChAT$^+$ (D) motor neurons per spinal cord ventral horn. Mean ± SEM, $N = 9$ $Fus^{+/+}$/*ChAT*-CRE, $N = 8$ $Fus^{\Delta NLS/\Delta NLS}$/−, and $N = 4$ $Fus^{\Delta NLS/\Delta NLS}$/*ChAT*-CRE for Nissl$^+$, and $N = 11$ $Fus^{+/+}$/*ChAT*-CRE, $N = 7$ $Fus^{\Delta NLS/\Delta NLS}$/−, and $N = 8$ $Fus^{\Delta NLS/\Delta NLS}$/*ChAT*-CRE for ChAT$^+$; (**) $P < 0.01$ versus $Fus^{+/+}$, $^{\#\#}P < 0.01$ versus $Fus^{\Delta NLS/+}$; (ns) non-significant; one-way ANOVA followed by Tukey's *post hoc* test.

E Total numbers of caspase-3 (Cas3)/ChAT/DAPI triple-positive cells in $Fus^{+/+}$/*ChAT*-CRE, $Fus^{\Delta NLS/\Delta NLS}$/−, and $Fus^{\Delta NLS/\Delta NLS}$/*ChAT*-CRE mice. $N = 9$ $Fus^{+/+}$/*ChAT*-CRE, $N = 7$ $Fus^{\Delta NLS/\Delta NLS}$/−, and $N = 8$ $Fus^{\Delta NLS/\Delta NLS}$/*ChAT*-CRE; $^{**}P < 0.01$ versus $Fus^{+/+}$, $^{\#}P < 0.05$ versus $Fus^{\Delta NLS/+}$; (ns) non-significant; one-way ANOVA followed by Tukey's *post hoc* test.

ChAT-CRE allele, suggesting that expression of mutant FUS in motor neurons is not the main contributor of neonatal lethality in homozygous mice. Last, we evaluated whether restoration of FUS nuclear localization in motor neurons would prevent motor neuron loss in $Fus^{\Delta NLS/\Delta NLS}$ mice. This approach revealed that the presence of a *ChAT*-CRE allele was indeed sufficient to fully rescue motor neuron loss (Fig 9B–D), as well as restore a normal number of caspase-3-positive motor neurons (Fig 9E). These findings establish that cytoplasmic FUS mislocalization within motor neurons is required to induce their loss in $Fus^{\Delta NLS/\Delta NLS}$ mice.

Discussion

FUS and other related RBPs form cytoplasmic inclusions associated with nuclear clearance in affected cells from ALS and FTD patients. An outstanding question is whether disease is caused by gain of cytoplasmic toxicity or by loss of the nuclear function of the respective RBP. To gain insight into this conundrum, we targeted the FUS locus to generate two novel mouse models. In the first model, the last exon of *Fus* is no longer transcribed, resulting in the production of a truncated FUS protein that lacks the NLS and localizes almost exclusively to the cytoplasm (Fig 1). The second model results in complete loss of FUS expression (Fig 3). A thorough comparison of these two models allowed us to determine whether a gain of a toxic cytoplasmic function is required for the observed phenotypes.

Interestingly, this approach revealed that $Fus^{\Delta NLS/\Delta NLS}$ and $Fus^{-/-}$ mice share several features: both mouse models die shortly after birth due to respiratory insufficiency and exhibit reduced body weight and size. Transcriptomic analysis also revealed overlapping alterations in RNA levels and splicing. However, a reduced number of spinal motor neurons associated with increased perinatal motor neuron apoptosis and a subset of expression and splicing changes were uniquely found in $Fus^{\Delta NLS/\Delta NLS}$ mice (Figs 4, 5, 6 and 7). Thus, FUS mislocalization to the cytoplasm with reduced levels of nuclear FUS is associated with phenotypes linked to loss of FUS function, but also with motor neuron death induced by a gain of toxicity mechanism that is not recapitulated in the knockout mouse model (Fig 6). The notion that loss of FUS function may not be sufficient to induce motor neuron degeneration is also supported by two recent reports. First, in an outbred genetic background, homozygous *Fus* gene trap mice reached 2 years of age without manifesting ALS-like phenotypes or motor neuron loss (Kino *et al*, 2015). Second, selective inactivation of the FUS homolog *cabeza* in neurons of adult *Drosophila* did not affect motor performance or life span, indicating that *cabeza* is not required for maintenance of neuronal function in adults (Frickenhaus *et al*, 2015). Here, we demonstrate that loss of FUS function is not sufficient and that gain of function by cytoplasmic redistribution of FUS is necessary to elicit motor neuron apoptosis. Notably, RNA-seq and RASL-seq experiments showed that the ΔNLS mutation triggered a partial loss of FUS function in splicing and gene expression regulation. Loss of function, although not sufficient, may be necessary in $Fus^{\Delta NLS/\Delta NLS}$ mice to induce motor neuron death. Indeed, a number of genes involved in synaptogenesis and/or in neurodegenerative diseases show altered expression (*Ahi1, Dmpk, Nefl, Nefm, Tuba4a, Taf15*) or splicing (*Ndrg2, Mapt, Atxn2, Sort1*) in $Fus^{\Delta NLS/\Delta NLS}$ and $Fus^{-/-}$ mice (Figs 4 and 5), and these alterations linked to loss of FUS nuclear function may weaken the motor neuron and sensitize it to the toxic effects of cytoplasmic FUS accumulation.

Importantly, we showed that motor neuron death in $Fus^{\Delta NLS/\Delta NLS}$ mice could be prevented by selectively restoring FUS nuclear import in motor neurons (Fig 9), demonstrating that FUS cytoplasmic mislocalization within motor neurons is required to induce motor neuron loss. The observation that cytoplasmic mislocalization of FUS is intrinsically toxic to motor neurons contrasts with the non-cell-autonomous contribution to motor neuron degeneration demonstrated for *SOD1* mutations (Boillee *et al*, 2006). Indeed, abrogation of mutant SOD1 expression in motor neurons delayed, but did not prevent, motor neuron degeneration, and a contribution of neighboring cells to SOD1 mediated toxicity is well established (Ilieva *et al*, 2009). Moreover, our data support a degenerative rather than developmental origin of motor neuron loss in newborn $Fus^{\Delta NLS/\Delta NLS}$ mice. The reduced number of motor neurons could have a developmental origin, either by impaired proliferation of motor neuron progenitors or defects in acquisition of motor neuron fate. However, this scenario is unlikely since motor neuron loss in $Fus^{\Delta NLS/\Delta NLS}$ mice can be prevented by ChAT-CRE-induced reversal of the $Fus^{\Delta NLS}$ locus to wild type (Fig 9). Expression of the ChAT gene, which encodes choline acetyl transferase, an enzyme essential for the biosynthesis of acetylcholine, is detectable in postmitotic motor neurons from E11.5 onwards, thus after exit from the cell cycle and acquisition of motor neuron fate at E.9.5 (Chen & Chiu, 1992; Alaynick *et al*, 2011; Cho *et al*, 2014). Therefore, the pathogenic events driving motor neuron loss in $Fus^{\Delta NLS/\Delta NLS}$ mice occur after motor neuron specification. It should be noted that a large proportion of motor neurons showed an incomplete rescue of FUS

nuclear localization. This could be either due to the rescue of one single allele or to the persistence of truncated FUS produced before CRE-mediated recombination. In any case, only a partial rescue of FUS subcellular localization was sufficient to abrogate motor neuron loss.

An attractive hypothesis to explain motor neuron loss in $Fus^{\Delta NLS/\Delta NLS}$ mice is that excessive motor neuron apoptosis happens during the so-called natural cell death period. During development, motor neurons are generated in excess and approximately 40% of the initially generated motor neurons are progressively removed. This process ensures the generation of the appropriate number of motor neurons and guarantees the elimination of motor neurons that did not establish proper neuromuscular junctions. According to the "neurotrophin hypothesis", developing motor neurons compete for limited amounts of neurotrophic factors produced by the muscle targets. Only motor axons that establish stable and functional neuromuscular junctions receive sufficient survival signals and are maintained (Oppenheim, 1991; Kanning *et al*, 2010). Importantly, we found that motor neuron loss elicited by cytoplasmic FUS mislocalization is associated with increased apoptosis of spinal motor neurons (Fig 7). Several motor neuron intrinsic mechanisms may underlie increased motor neuron apoptosis in $Fus^{\Delta NLS/\Delta NLS}$ mice and future studies are needed to investigate these possible mechanisms. For instance, expression of axon guidance receptors may be deregulated in $Fus^{\Delta NLS/\Delta NLS}$ mice, leading to defects in motor axon targeting and failure to receive neurotrophic support. Alternatively, $Fus^{\Delta NLS/\Delta NLS}$ motor axons may reach their targets, but reduced expression of receptors for muscle-derived neurotrophic factors may render a fraction of motor neurons insensitive to survival signals.

Previous work suggested various potential toxic mechanisms for cytoplasmic FUS, and our study sheds light on several of these candidate pathways. First, cytoplasmic FUS could generate toxic FUS aggregates in the cytosol, as shown in yeast models of FUSopathies (Ju *et al*, 2011; Sun *et al*, 2011). Here, we detected neither FUS-positive nor ubiquitin-positive aggregates expected to occur in case of strong ubiquitin proteasome system (UPS) impairment. Thus, at least in this model and at this perinatal age, FUS aggregation or robust FUS-mediated impairment of protein clearance pathways is dispensable for toxicity toward motor neurons. Cytoplasmic FUS could also alter stress granule (SG) dynamics through its localization to SGs upon stress and its regulatory properties toward SG assembly (Li *et al*, 2013). In $Fus^{\Delta NLS/\Delta NLS}$ mice, we did not observe formation of SGs in spinal cord motor neurons using TIAR as a marker, suggesting that major impairment of SG biology is not required for FUS toxicity *in vivo* in this model. However, we observed increased phosphorylation of the translation initiation factor eIF2α, an event known to be caused by cellular stress and to lead to repression of global protein translation (Holcik & Sonenberg, 2005; Sonenberg & Hinnebusch, 2009). Consistent with this scenario, gene ontology analysis of differentially expressed genes also pointed to alterations in mRNA translation as a potential function uniquely altered in $Fus^{\Delta NLS/\Delta NLS}$ mice.

In addition to increased eIF2α phosphorylation, several FUS binding partners are affected in their subcellular localization upon cytoplasmic FUS mislocalization. Firstly, SMN1-positive nuclear gems were lost in $Fus^{\Delta NLS/\Delta NLS}$ motor neurons, likely as a consequence of FUS loss of function, as FUS was shown to be required for gem formation in HeLa cells and primary hippocampal neurons (Yamazaki *et al*, 2012; Tsuiji *et al*, 2013). Intriguingly, nuclear gems were also reduced in fibroblasts from ALS patients with FUS or TDP-43 mutations, and in motor neurons in postmortem lumbar spinal cord from ALS patients (Yamazaki *et al*, 2012; Tsuiji *et al*, 2013; Sun *et al*, 2015). Furthermore, we observed a dramatic concentration of HDAC1 in nuclear foci in $Fus^{\Delta NLS/\Delta NLS}$ neurons. The exact consequences of this abnormal HDAC1 localization remain to be determined, but the pleiotropic functions of HDAC1 in cell survival, axonal damage, and repair of DNA damage (Kim *et al*, 2010; Wang *et al*, 2013) suggest that downstream consequences of abnormal HDAC1 distribution might underlie toxicity. In any case, the abnormal subcellular localizations of HDAC1 and SMN in $Fus^{\Delta NLS/\Delta NLS}$ neurons provide evidence that FUS cytoplasmic mislocalization could lead to alterations in splicing or gene expression through cytoplasmic retention or abnormal trafficking of its interaction partners.

An interesting observation is that both $Fus^{\Delta NLS/\Delta NLS}$ and $Fus^{-/-}$ mice die shortly after birth of respiratory insufficiency, presumably caused by loss of FUS function. A concerted action of several physiological systems is required for newborn mice to breathe normally, and defects in any of these systems can lead to neonatal lethality (Turgeon & Meloche, 2009). Firstly, the respiratory rhythm is generated in the respiratory center in the brainstem and transmitted through the spinal motor neurons to the respiratory muscles (diaphragm and intercostals muscles). Therefore, structural or functional defects of neurons in the respiratory center, motor neurons, neuromuscular junctions, and/or respiratory muscles can lead to respiratory distress. Our observation that neonatal lethality of $Fus^{\Delta NLS/\Delta NLS}$ mice is not rescued by restoration of FUS nuclear import in motor neurons indicates that loss of FUS function in cell types other than motor neurons is sufficient to trigger neonatal lethality. Alternatively, the expression of CRE under the *ChAT* promoter may occur too late in the development to provide a complete rescue of the motor neurons functionality. The remaining cytoplasmic FUS observed in rescued motor neurons could result either from a long half-life of FUS protein in motor neurons or from CRE-mediated recombination of only one allele. Thus, rescued motor neurons, despite being histologically normal, could remain functionally altered due to residual cytoplasmic FUS. This would be analogous to results observed in Nova double knockout animals rescued with neuronal agrin (Ruggiu *et al*, 2009). Electrophysiological characterization of neuromuscular transmission could help discriminate between these two possibilities. Apart from neuromuscular alterations, defects in lung morphogenesis or maturation, cardiovascular defects, hematological defects, or skeletal defects can all result in poor blood oxygenation and the characteristic cyanosis observed in $Fus^{\Delta NLS/\Delta NLS}$ and $Fus^{-/-}$ neonates. It will be important to investigate these possible causes of neonatal lethality due to loss of FUS function in future studies. In particular, generation of conditional *Fus* knockout mice would provide a valuable tool to evaluate whether selective FUS inactivation in neurons, muscle, lung epithelium, or the vasculature would result in respiratory insufficiency and neonatal death. Possibly, loss of FUS function in a combination of these tissues is necessary to induce this phenotype.

While a few FUS mutations have a recessive pattern of inheritance (Kwiatkowski *et al*, 2009; Bertolin *et al*, 2014), the vast majority are dominantly inherited, and most ALS patients are affected in

their 5th to 7th decade. Thus, our observation of perinatal death is not fully representative of the disease state as occurs in ALS patients and some changes observed here might be deleterious through developmental rather than degenerative effects. In this respect, it will be crucial to further analyze heterozygous $Fus^{\Delta NLS/+}$ mice that closely mimic the genetic situation in the vast majority of ALS-FUS patients. These mice are viable and show no obvious motor phenotype until 6 months of age (Scekic-Zahirovic, unpublished results). Nevertheless, $Fus^{\Delta NLS/+}$ mice showed cytoplasmic mislocalization of FUS and subtle alterations in mRNA splicing at birth. Aging might exacerbate these defects, consistent with a late-onset disease such as ALS, and it will be highly interesting to characterize a potential age-dependent phenotype of $Fus^{\Delta NLS/+}$ mice and $Fus^{+/-}$ mice.

The very severe phenotype of $Fus^{\Delta NLS/\Delta NLS}$ mice resembles spinal muscular atrophy, which is caused by mutations in the *SMN1* gene, whose product SMN interacts directly with FUS and is an integral component of the spliceosome (Yamazaki *et al*, 2012; Gerbino *et al*, 2013; Groen *et al*, 2013; Tsuiji *et al*, 2013; Sun *et al*, 2015; Yu *et al*, 2015). This is further reinforced by the strong splicing defects observed in $Fus^{\Delta NLS/\Delta NLS}$ mice and is consistent with juvenile onset in many ALS-*FUS* patients with C-terminal truncation mutations. These similarities strengthen the links between ALS and SMA, and support that SMA, ALS, and FTD may be part of the same disease spectrum with common molecular mechanisms leading to neuronal death.

In conclusion, this study provides *in vivo* genetic evidence that cytoplasmic mislocalization of FUS triggers apoptotic motor neuron degeneration and demonstrates a crucial role for a gain of toxic function in this process. Motor neuron loss occurs at least partially through a cell autonomous gain-of-function mechanism, since complete loss of FUS is not associated with motor neuron death, and rescue of nuclear FUS within motor neurons prevents neuronal death.

Materials and Methods

Generation of conditional knockin $Fus^{\Delta NLS/\Delta NLS}$ and $Fus^{-/-}$ mice

Knockin *Fus* mice with the conditional ablation of exon 15 were generated in the Institut Clinique de la Souris (ICS, Illkirch, Strasbourg) using standard procedures. The *Fus* locus was engineered to include, in between the exons 12 and 13 of the gene, an inserted floxed cDNA encoding exons 13 and 14 of *FUS*, followed by 3 STOP cassettes. We obtained germ line transmission of the recombinant allele. Homozygous $Fus^{\Delta NLS/\Delta NLS}$ mice were generated by intercrossing $Fus^{\Delta NLS/+}$ animals.

For generation of $Fus^{-/-}$ mice, the mouse ES cell clone EUCE0131_G08 was obtained from the European Conditional Mouse Mutagenesis Consortium (EUCOMM) (Friedel *et al*, 2007). Southern blotting and sequencing of PCR-amplified genomic sequences confirmed a single gene trap insertion event in the first intron of *Fus*. Blastocyst injection of ES cells resulted in chimeric mice, which allowed for germ line transmission of the mutant *Fus* allele. As the ES cells were generated in a 129P2 background, the resulting offspring was backcrossed at least five times to C57Bl6 mice. The genetic background of all mice used in this study is C57Bl6.

Western blot

Western blotting and antibodies used are presented in Appendix Supplementary Methods.

Histology and motor neuron counts

Spinal cords were removed and immersed in fixative for 2 h at 4°C. Samples were transferred overnight into 30% sucrose in 0.1 M phosphate buffer (PB) at 4°C for cryoprotection, embedded in medium (Tissue-Tek® O.C.T. Compound, SAKURA#4583), and cut with a cryostat (Leica CM 3050S). P0 spinal cords were cut in serial 25-μm-thick sections and mounted onto 2% gelatin-coated slides to be processed for immunostaining.

For Nissl staining, slides were air-dried overnight. Sections were then hydrated through 100% and 95% alcohol to distilled water, immersed in 0.1% Cresyl violet acetate (Certistain®, MERCK#5235), and coverslipped with Roti-Histokitt (Roth, 6638.1).

For immunohistochemistry (IHC), unspecific binding sites were blocked with 5% horse serum (HS), 0.5% Triton X-100 for 30 min at room temperature (RT), immersed in 3% hydrogen peroxide (H_2O_2) to remove the endogenous peroxidase activity, rinsed in phosphate buffered saline (PBS), and incubated with goat polyclonal anti-choline acetyltransferase (ChAT) antibody (Millipore, AB144-P; diluted 1:50) overnight at RT in a humidified chamber. After rinsing in PBS, sections were incubated with biotinylated donkey anti-goat IgG (Jackson, 705-066-147; 1:250) for 1.5 h, rinsed in PBS, and then incubated with ABC kit (Vector, PK7200; 1:4,000) for 1 h. All antibodies were diluted in 0.01 M PBS, 0.1% Triton X-100. Peroxidase staining was obtained by incubating the sections in 0.075% 3,3′-diaminobenzidine tetrahydrochloride (DAB; Sigma Aldrich) and 0.002% H_2O_2 in 50 mM Tris–HCl pH 7.5. Sections were dehydrated, air-dried, and coverslipped with Roti-Histokitt (Roth, 6638.1).

Motor neurons were counted at L1–L5 on both cresyl violet- and ChAT-stained sections at 20× magnification (for each genotype: Exact numbers of animals per group are provided in figure legends). The counting was performed per ventral horn in every tenth section for ten sections in total per animal. In Nissl-stained sections, only neurons with an area ≥ 80 μm^2 and located in a position congruent with that of motor neuron groups were counted (d'Errico *et al*, 2013). All $ChAT^+$ profiles located in the ventral horns of immunostained sections clearly displayed on the plane of the section were counted. Total estimated motor neuron numbers were obtained using a computer-assisted microscope (Nikon Eclipse E800) and the software (Nis Elements version 4.0). Cells were counted on the computer screen using a digital camera (Nikon Digital Sight DS-U3) mounted on a microscope. The soma size of Nissl+ motor neurons was also analyzed by measuring cross-sectional areas at 20× magnification using ImageJ software (Schneider *et al*, 2012).

Other histological techniques are described in Appendix Supplementary Methods.

Analysis of expression changes by RNA-seq

Total RNA from brains of $Fus^{\Delta NLS/\Delta NLS}$, $Fus^{-/-}$, and their control littermates were extracted with TRIzol (Invitrogen). RNA quality was measured using the Agilent Bioanalyzer system or RNA ScreenTape (Agilent technologies) according to the manufacturer's

recommendations and processed using the Illumina TruSeq Stranded mRNA Sample Preparation Kit according to manufacturer's protocol. Generated cDNA libraries were sequenced using an Illumina HiSeq 2000 sequencer with 4–5 biological replicates sequenced per condition using single read, 50 cycle runs. Quality of sequencing reads was assessed using FastQC (Babraham Bioinformatics) and then aligned to a mouse reference genome (mm9, UCSC Genome Browser) using TopHat (version v2.0.10). Sequencing yielded, on average, 15 million non-redundant reads per sample with a 48.4–58.7% mapping rate. Cufflinks (version v2.1.1) was used to generate transcript abundance for each annotated protein-coding gene as fragments per kilobase of transcript per million mapped reads (FPKM), and statistical analysis and comparison of FPKM values were calculated using Cuffdiff (version v2.1.1). Genomewide unsupervised clustering analysis and heat maps with significant changes between different groups were generated using R (Bioconductor). qRT–PCR techniques used to confirm RNA-seq changes are described in Appendix Supplementary Methods and oligonucleotides sequences are provided in Dataset EV9.

Analysis of splicing alterations by RASL-seq

RNA-mediated oligonucleotide annealing, selection, and ligation with next-generation sequencing (RASL-seq) analysis of alternative splicing changes was carried out as already described elsewhere (Li *et al*, 2012; Zhou *et al*, 2012). In brief, a pool of oligonucleotides was designed to detect 3,859 alternative splicing events in mice. One hundred fmol of RASL-seq oligos were annealed to 1 μg of total RNA isolated from brains of $Fus^{\Delta NLS/\Delta NLS}$, $Fus^{-/-}$, and their control littermates. After ligation, 5 μl eluted ligated oligos were used for 16–18 cycles of PCR amplification, and the barcoded PCR products were sequenced using an Illumina HiSeq 2000 sequencer with 24–30 samples per lanes. Sequencing data were decoded allowing no mismatch with each barcode, and target sequences were mapped with RASL-seq oligo pool sequences using the short read alignment software Bowtie allowing for 1 mismatch at both the left and right side of the ligated oligos. An average of ~5 million reads from each sample was mapped, with events with < 4 counts in one of the isoforms removed. Ratios of the counts of shorter to longer isoforms were calculated. The significantly changed events were identified by *t*-test and average fold change. Unsupervised clustering analysis and heat maps with significant changes between different groups were generated using R (Bioconductor). Semi-quantitative PCR techniques used to confirm RASL-seq changes are described in Appendix Supplementary Methods. Oligonucleotides sequences are provided in Dataset EV9.

Statistics

For the animal experiments, the values from each animal were averaged for each genotype group and analyzed by Student's unpaired two-tailed *t*-test. Comparison of three or four groups was performed using one-way ANOVA and Tukey's *post hoc* test. Data were analyzed by using the Graphics Prism Program (Graph Pad Software, San Diego, CA) and expressed as mean ± SEM (standard error of the mean) and differences were considered significant when $P \leq 0.05$.

Data accession

RNA-seq and RASL-seq data have been deposited in GEO, under entry GSE78730.

Expanded View for this article is available online.

Acknowledgements
We thank Dr. Pico Caroni for providing the ChAT-CRE knockin mice and helpful discussions. We thank Marlene Bartos for her help in achieving this project. We are grateful to Dr. Don W. Cleveland and the members of his group for tremendous support and fruitful discussions. This work is supported by an ALS Association Investigator Initiated Award (grants 2235 and 3209; to LD and CLT); the Frick Foundation (award 2013 to LD and CLT, award 2010 to ES); Association Française contre les Myopathies (grant #18280; to LD, CLT and ES); Target ALS (grant 13-0840; to CLT); Virtual Helmholtz Institute "RNA dysmetabolism in ALS and FTD" (WP2, to LD, AW and ACL); Association de recherche sur la SLA (ArSLA; to LD); State North Rhine Westphalia (to ES); Minna-James-Heineman-Stiftung (to ES); and the Max Planck Society (to ES). JSZ received a Erasmus Mundus Neurotime Fellowship to perform these studies. OS received a fellowship from the German National Academic Foundation. CLT received salary support from the Ludwig Institute for Cancer Research.

Author contributions
JSZ, OS, ES, CLT, and LD designed research; JSZ, OS, HEO, MJ, SM, MW, SD, JS, SDG, KD, NM, MCB, JQ, CR, TS, and ES performed research; SY, JQ, YZ, HL, XDF, AW, ACL, and FK contributed reagents and data analysis; JSZ, OS, MJ, SY, KD, ES, CLT, and LD analyzed data and made figures; and JSZ, ES, CLT, and LD wrote the manuscript.

Conflict of interest
The authors declare that they have no conflict of interest.

References

Alami NH, Smith RB, Carrasco MA, Williams LA, Winborn CS, Han SS, Kiskinis E, Winborn B, Freibaum BD, Kanagaraj A, Clare AJ, Badders NM, Bilican B, Chaum E, Chandran S, Shaw CE, Eggan KC, Maniatis T, Taylor JP (2014) Axonal transport of TDP-43 mRNA granules is impaired by ALS-causing mutations. *Neuron* 81: 536 – 543

Alaynick WA, Jessell TM, Pfaff SL (2011) SnapShot: spinal cord development. *Cell* 146: 178 – 178 e1

Arnold ES, Ling SC, Huelga SC, Lagier-Tourenne C, Polymenidou M, Ditsworth D, Kordasiewicz HB, McAlonis-Downes M, Platoshyn O, Parone PA, Da Cruz S, Clutario KM, Swing D, Tessarollo L, Marsala M, Shaw CE, Yeo GW, Cleveland DW (2013) ALS-linked TDP-43 mutations produce aberrant RNA splicing and adult-onset motor neuron disease without aggregation or loss of nuclear TDP-43. *Proc Natl Acad Sci USA* 110: E736 – E745

Ayala YM, De Conti L, Avendano-Vazquez SE, Dhir A, Romano M, D'Ambrogio A, Tollervey J, Ule J, Baralle M, Buratti E, Baralle FE (2011) TDP-43 regulates its mRNA levels through a negative feedback loop. *EMBO J* 30: 277 – 288

Baumer D, Hilton D, Paine SM, Turner MR, Lowe J, Talbot K, Ansorge O (2010) Juvenile ALS with basophilic inclusions is a FUS proteinopathy with FUS mutations. *Neurology* 75: 611 – 618

Bergeron C, Beric-Maskarel K, Muntasser S, Weyer L, Somerville MJ, Percy ME (1994) Neurofilament light and polyadenylated mRNA levels are decreased

in amyotrophic lateral sclerosis motor neurons. *J Neuropathol Exp Neurol* 53: 221 – 230

Bertolin C, D'Ascenzo C, Querin G, Gaiani A, Boaretto F, Salvoro C, Vazza G, Angelini C, Cagnin A, Pegoraro E, Soraru G, Mostacciuolo ML (2014) Improving the knowledge of amyotrophic lateral sclerosis genetics: novel SOD1 and FUS variants. *Neurobiol Aging* 35: 1212 e7 – 1212 e10.

Boillee S, Vande Velde C, Cleveland DW (2006) ALS: a disease of motor neurons and their nonneuronal neighbors. *Neuron* 52: 39 – 59

Calvo A, Moglia C, Canosa A, Brunetti M, Barberis M, Traynor BJ, Carrara G, Valentini C, Restagno G, Chio A (2014) *De novo* nonsense mutation of the FUS gene in an apparently familial amyotrophic lateral sclerosis case. *Neurobiol Aging* 35: 1513 e7 – 11

Cambray S, Pedraza N, Rafel M, Gari E, Aldea M, Gallego C (2009) Protein kinase KIS localizes to RNA granules and enhances local translation. *Mol Cell Biol* 29: 726 – 735

Chen EW, Chiu AY (1992) Early stages in the development of spinal motor neurons. *J Comp Neurol* 320: 291 – 303

Cho HH, Cargnin F, Kim Y, Lee B, Kwon RJ, Nam H, Shen R, Barnes AP, Lee JW, Lee S, Lee SK (2014) Isl1 directly controls a cholinergic neuronal identity in the developing forebrain and spinal cord by forming cell type-specific complexes. *PLoS Genet* 10: e1004280

Couthouis J, Hart MP, Shorter J, DeJesus-Hernandez M, Erion R, Oristano R, Liu AX, Ramos D, Jethava N, Hosangadi D, Epstein J, Chiang A, Diaz Z, Nakaya T, Ibrahim F, Kim HJ, Solski JA, Williams KL, Mojsilovic-Petrovic J, Ingre C *et al* (2011) A yeast functional screen predicts new candidate ALS disease genes. *Proc Natl Acad Sci USA* 108: 20881 – 20890

Couthouis J, Hart MP, Erion R, King OD, Diaz Z, Nakaya T, Ibrahim F, Kim HJ, Mojsilovic-Petrovic J, Panossian S, Kim CE, Frackelton EC, Solski JA, Williams KL, Clay-Falcone D, Elman L, McCluskey L, Greene R, Hakonarson H, Kalb RG *et al* (2012) Evaluating the role of the FUS/TLS-related gene EWSR1 in amyotrophic lateral sclerosis. *Hum Mol Genet* 21: 2899 – 2911

D'Alton S, Altshuler M, Lewis J (2015) Studies of alternative isoforms provide insight into TDP-43 autoregulation and pathogenesis. *RNA* 21: 1419 – 1432

Deng H, Gao K, Jankovic J (2014) The role of FUS gene variants in neurodegenerative diseases. *Nat Rev Neurol* 10: 337 – 348

Dillman AA, Hauser DN, Gibbs JR, Nalls MA, McCoy MK, Rudenko IN, Galter D, Cookson MR (2013) mRNA expression, splicing and editing in the embryonic and adult mouse cerebral cortex. *Nat Neurosci* 16: 499 – 506

Dini Modigliani S, Morlando M, Errichelli L, Sabatelli M, Bozzoni I (2014) An ALS-associated mutation in the FUS 3′-UTR disrupts a microRNA-FUS regulatory circuitry. *Nat Commun* 5: 4335

Dormann D, Rodde R, Edbauer D, Bentmann E, Fischer I, Hruscha A, Than ME, Mackenzie IR, Capell A, Schmid B, Neumann M, Haass C (2010) ALS-associated fused in sarcoma (FUS) mutations disrupt Transportin-mediated nuclear import. *EMBO J* 29: 2841 – 2857

Elden AC, Kim HJ, Hart MP, Chen-Plotkin AS, Johnson BS, Fang X, Armakola M, Geser F, Greene R, Lu MM, Padmanabhan A, Clay-Falcone D, McCluskey L, Elman L, Juhr D, Gruber PJ, Rub U, Auburger G, Trojanowski JQ, Lee VM *et al* (2010) Ataxin-2 intermediate-length polyglutamine expansions are associated with increased risk for ALS. *Nature* 466: 1069 – 1075

d'Errico P, Boido M, Piras A, Valsecchi V, De Amicis E, Locatelli D, Capra S, Vagni F, Vercelli A, Battaglia G (2013) Selective vulnerability of spinal and cortical motor neuron subpopulations in delta7 SMA mice. *PLoS ONE* 8: e82654

Ferland RJ, Eyaid W, Collura RV, Tully LD, Hill RS, Al-Nouri D, Al-Rumayyan A, Topcu M, Gascon G, Bodell A, Shugart YY, Ruvolo M, Walsh CA (2004) Abnormal cerebellar development and axonal decussation due to mutations in AHI1 in Joubert syndrome. *Nat Genet* 36: 1008 – 1013

Frickenhaus M, Wagner M, Mallik M, Catinozzi M, Storkebaum E (2015) Highly efficient cell-type-specific gene inactivation reveals a key function for the Drosophila FUS homolog cabeza in neurons. *Sci Rep* 5: 9107

Friedel RH, Seisenberger C, Kaloff C, Wurst W (2007) EUCOMM–the European conditional mouse mutagenesis program. *Brief Funct Genomic Proteomic* 6: 180 – 185

Gerbino V, Carri MT, Cozzolino M, Achsel T (2013) Mislocalised FUS mutants stall spliceosomal snRNPs in the cytoplasm. *Neurobiol Dis* 55: 120 – 128

Gitcho MA, Baloh RH, Chakraverty S, Mayo K, Norton JB, Levitch D, Hatanpaa KJ, White CL III, Bigio EH, Caselli R, Baker M, Al-Lozi MT, Morris JC, Pestronk A, Rademakers R, Goate AM, Cairns NJ (2008) TDP-43 A315T mutation in familial motor neuron disease. *Ann Neurol* 63: 535 – 538

Groen EJ, Fumoto K, Blokhuis AM, Engelen-Lee J, Zhou Y, van den Heuvel DM, Koppers M, van Diggelen F, van Heest J, Demmers JA, Kirby J, Shaw PJ, Aronica E, Spliet WG, Veldink JH, van den Berg LH, Pasterkamp RJ (2013) ALS-associated mutations in FUS disrupt the axonal distribution and function of SMN. *Hum Mol Genet* 22: 3690 – 3704

Han TW, Kato M, Xie S, Wu LC, Mirzaei H, Pei J, Chen M, Xie Y, Allen J, Xiao G, McKnight SL (2012) Cell-free formation of RNA granules: bound RNAs identify features and components of cellular assemblies. *Cell* 149: 768 – 779

Hicks GG, Singh N, Nashabi A, Mai S, Bozek G, Klewes L, Arapovic D, White EK, Koury MJ, Oltz EM, Van Kaer L, Ruley HE (2000) Fus deficiency in mice results in defective B-lymphocyte development and activation, high levels of chromosomal instability and perinatal death. *Nat Genet* 24: 175 – 179

Holcik M, Sonenberg N (2005) Translational control in stress and apoptosis. *Nat Rev Mol Cell Biol* 6: 318 – 327

Hu F, Padukkavidana T, Vaegter CB, Brady OA, Zheng Y, Mackenzie IR, Feldman HH, Nykjaer A, Strittmatter SM (2010) Sortilin-mediated endocytosis determines levels of the frontotemporal dementia protein, progranulin. *Neuron* 68: 654 – 667

Huang EJ, Zhang J, Geser F, Trojanowski JQ, Strober JB, Dickson DW, Brown RH Jr, Shapiro BE, Lomen-Hoerth C (2010) Extensive FUS-immunoreactive pathology in juvenile amyotrophic lateral sclerosis with basophilic inclusions. *Brain Pathol* 20: 1069 – 1076

Huang C, Zhou H, Tong J, Chen H, Liu YJ, Wang D, Wei X, Xia XG (2011) FUS transgenic rats develop the phenotypes of amyotrophic lateral sclerosis and frontotemporal lobar degeneration. *PLoS Genet* 7: e1002011

Hutton M, Lendon CL, Rizzu P, Baker M, Froelich S, Houlden H, Pickering-Brown S, Chakraverty S, Isaacs A, Grover A, Hackett J, Adamson J, Lincoln S, Dickson D, Davies P, Petersen RC, Stevens M, de Graaff E, Wauters E, van Baren J *et al* (1998) Association of missense and 5′-splice-site mutations in tau with the inherited dementia FTDP-17. *Nature* 393: 702 – 705

Ilieva H, Polymenidou M, Cleveland DW (2009) Non-cell autonomous toxicity in neurodegenerative disorders: ALS and beyond. *J Cell Biol* 187: 761 – 772

Imbert G, Saudou F, Yvert G, Devys D, Trottier Y, Garnier JM, Weber C, Mandel JL, Cancel G, Abbas N, Durr A, Didierjean O, Stevanin G, Agid Y, Brice A (1996) Cloning of the gene for spinocerebellar ataxia 2 reveals a locus with high sensitivity to expanded CAG/glutamine repeats. *Nat Genet* 14: 285 – 291

Ishigaki S, Masuda A, Fujioka Y, Iguchi Y, Katsuno M, Shibata A, Urano F, Sobue G, Ohno K (2012) Position-dependent FUS-RNA interactions regulate alternative splicing events and transcriptions. *Sci Rep* 2: 529

Johnson JO, Pioro EP, Boehringer A, Chia R, Feit H, Renton AE, Pliner HA, Abramzon Y, Marangi G, Winborn BJ, Gibbs JR, Nalls MA, Morgan S, Shoai M, Hardy J, Pittman A, Orrell RW, Malaspina A, Sidle KC, Fratta P *et al* (2014) Mutations in the Matrin 3 gene cause familial amyotrophic lateral sclerosis. *Nat Neurosci* 17: 664 – 666

Ju S, Tardiff DF, Han H, Divya K, Zhong Q, Maquat LE, Bosco DA, Hayward LJ, Brown RH Jr, Lindquist S, Ringe D, Petsko GA (2011) A yeast model of FUS/TLS-dependent cytotoxicity. *PLoS Biol* 9: e1001052

Kabashi E, Valdmanis PN, Dion P, Spiegelman D, McConkey BJ, Vande Velde C, Bouchard JP, Lacomblez L, Pochigaeva K, Salachas F, Pradat PF, Camu W, Meininger V, Dupre N, Rouleau GA (2008) TARDBP mutations in individuals with sporadic and familial amyotrophic lateral sclerosis. *Nat Genet* 40: 572 – 574

Kanning KC, Kaplan A, Henderson CE (2010) Motor neuron diversity in development and disease. *Annu Rev Neurosci* 33: 409 – 440

Kim JY, Shen S, Dietz K, He Y, Howell O, Reynolds R, Casaccia P (2010) HDAC1 nuclear export induced by pathological conditions is essential for the onset of axonal damage. *Nat Neurosci* 13: 180 – 189

Kim HJ, Kim NC, Wang YD, Scarborough EA, Moore J, Diaz Z, MacLea KS, Freibaum B, Li S, Molliex A, Kanagaraj AP, Carter R, Boylan KB, Wojtas AM, Rademakers R, Pinkus JL, Greenberg SA, Trojanowski JQ, Traynor BJ, Smith BN *et al* (2013) Mutations in prion-like domains in hnRNPA2B1 and hnRNPA1 cause multisystem proteinopathy and ALS. *Nature* 495: 467 – 473

Kino Y, Washizu C, Kurosawa M, Yamada M, Miyazaki H, Akagi T, Hashikawa T, Doi H, Takumi T, Hicks GG, Hattori N, Shimogori T, Nukina N (2015) FUS/TLS deficiency causes behavioral and pathological abnormalities distinct from amyotrophic lateral sclerosis. *Acta Neuropathol Commun* 3: 24

Kobayashi Z, Tsuchiya K, Arai T, Aoki M, Hasegawa M, Ishizu H, Akiyama H, Mizusawa H (2010) Occurrence of basophilic inclusions and FUS-immunoreactive neuronal and glial inclusions in a case of familial amyotrophic lateral sclerosis. *J Neurol Sci* 293: 6 – 11

Kuroda M, Sok J, Webb L, Baechtold H, Urano F, Yin Y, Chung P, de Rooij DG, Akhmedov A, Ashley T, Ron D (2000) Male sterility and enhanced radiation sensitivity in TLS(−/−) mice. *EMBO J* 19: 453 – 462

Kwiatkowski TJ Jr, Bosco DA, Leclerc AL, Tamrazian E, Vanderburg CR, Russ C, Davis A, Gilchrist J, Kasarskis EJ, Munsat T, Valdmanis P, Rouleau GA, Hosler BA, Cortelli P, de Jong PJ, Yoshinaga Y, Haines JL, Pericak-Vance MA, Yan J, Ticozzi N *et al* (2009) Mutations in the FUS/TLS gene on chromosome 16 cause familial amyotrophic lateral sclerosis. *Science* 323: 1205 – 1208

Lagier-Tourenne C, Polymenidou M, Hutt KR, Vu AQ, Baughn M, Huelga SC, Clutario KM, Ling SC, Liang TY, Mazur C, Wancewicz E, Kim AS, Watt A, Freier S, Hicks GG, Donohue JP, Shiue L, Bennett CF, Ravits J, Cleveland DW *et al* (2012) Divergent roles of ALS-linked proteins FUS/TLS and TDP-43 intersect in processing long pre-mRNAs. *Nat Neurosci* 15: 1488 – 1497

Li H, Qiu J, Fu XD (2012) RASL-seq for massively parallel and quantitative analysis of gene expression. *Curr Protocols Mol Biol*/edited by Ausubel FM, Brent R, Kingston RE, Moore DD, Seidman JG, Smith JA, Struhl K. Chapter 4: Unit 4.13.1 – 9

Li YR, King OD, Shorter J, Gitler AD (2013) Stress granules as crucibles of ALS pathogenesis. *J Cell Biol* 201: 361 – 372

Ling SC, Polymenidou M, Cleveland DW (2013) Converging mechanisms in ALS and FTD: disrupted RNA and protein homeostasis. *Neuron* 79: 416 – 438

Ling JP, Pletnikova O, Troncoso JC, Wong PC (2015) TDP-43 repression of nonconserved cryptic exons is compromised in ALS-FTD. *Science* 349: 650 – 655

Liu F, Gong CX (2008) Tau exon 10 alternative splicing and tauopathies. *Mol Neurodegener* 3: 8

Liu-Yesucevitz L, Bilgutay A, Zhang YJ, Vanderweyde T, Citro A, Mehta T, Zaarur N, McKee A, Bowser R, Sherman M, Petrucelli L, Wolozin B (2010) Tar DNA binding protein-43 (TDP-43) associates with stress granules: analysis of cultured cells and pathological brain tissue. *PLoS ONE* 5: e13250

Mackenzie IR, Rademakers R, Neumann M (2010) TDP-43 and FUS in amyotrophic lateral sclerosis and frontotemporal dementia. *Lancet Neurol* 9: 995 – 1007

Manceau V, Kielkopf CL, Sobel A, Maucuer A (2008) Different requirements of the kinase and UHM domains of KIS for its nuclear localization and binding to splicing factors. *J Mol Biol* 381: 748 – 762

McMillan P, Korvatska E, Poorkaj P, Evstafjeva Z, Robinson L, Greenup L, Leverenz J, Schellenberg GD, D'Souza I (2008) Tau isoform regulation is region- and cell-specific in mouse brain. *J Comp Neurol* 511: 788 – 803

Mitchell JC, McGoldrick P, Vance C, Hortobagyi T, Sreedharan J, Rogelj B, Tudor EL, Smith BN, Klasen C, Miller CC, Cooper JD, Greensmith L, Shaw CE (2013) Overexpression of human wild-type FUS causes progressive motor neuron degeneration in an age- and dose-dependent fashion. *Acta Neuropathol* 125: 273 – 288

Mitchelmore C, Buchmann-Moller S, Rask L, West MJ, Troncoso JC, Jensen NA (2004) NDRG2: a novel Alzheimer's disease associated protein. *Neurobiol Dis* 16: 48 – 58

Morlando M, Dini Modigliani S, Torrelli G, Rosa A, Di Carlo V, Caffarelli E, Bozzoni I (2012) FUS stimulates microRNA biogenesis by facilitating co-transcriptional Drosha recruitment. *EMBO J* 31: 4502 – 4510

Mortazavi A, Williams BA, McCue K, Schaeffer L, Wold B (2008) Mapping and quantifying mammalian transcriptomes by RNA-Seq. *Nat Methods* 5: 621 – 628

Neumann M, Sampathu DM, Kwong LK, Truax AC, Micsenyi MC, Chou TT, Bruce J, Schuck T, Grossman M, Clark CM, McCluskey LF, Miller BL, Masliah E, Mackenzie IR, Feldman H, Feiden W, Kretzschmar HA, Trojanowski JQ, Lee VM (2006) Ubiquitinated TDP-43 in frontotemporal lobar degeneration and amyotrophic lateral sclerosis. *Science* 314: 130 – 133

Neumann M, Rademakers R, Roeber S, Baker M, Kretzschmar HA, Mackenzie IR (2009) A new subtype of frontotemporal lobar degeneration with FUS pathology. *Brain* 132: 2922 – 2931

Oppenheim RW (1991) Cell death during development of the nervous system. *Annu Rev Neurosci* 14: 453 – 501

Parkhomchuk D, Borodina T, Amstislavskiy V, Banaru M, Hallen L, Krobitsch S, Lehrach H, Soldatov A (2009) Transcriptome analysis by strand-specific sequencing of complementary DNA. *Nucleic Acids Res* 37: e123

Pedraza N, Ortiz R, Cornado A, Llobet A, Aldea M, Gallego C (2014) KIS, a kinase associated with microtubule regulators, enhances translation of AMPA receptors and stimulates dendritic spine remodeling. *J Neurosci* 34: 13988 – 13997

Polymenidou M, Lagier-Tourenne C, Hutt KR, Huelga SC, Moran J, Liang TY, Ling SC, Sun E, Wancewicz E, Mazur C, Kordasiewicz H, Sedaghat Y, Donohue JP, Shiue L, Bennett CF, Yeo GW, Cleveland DW (2011) Long pre-mRNA depletion and RNA missplicing contribute to neuronal vulnerability from loss of TDP-43. *Nat Neurosci* 14: 459 – 468

Prudencio M, Jansen-West KR, Lee WC, Gendron TF, Zhang YJ, Xu YF, Gass J, Stuani C, Stetler C, Rademakers R, Dickson DW, Buratti E, Petrucelli L (2012) Misregulation of human sortilin splicing leads to the generation of a nonfunctional progranulin receptor. *Proc Natl Acad Sci USA* 109: 21510 – 21515

Rogelj B, Easton LE, Bogu GK, Stanton LW, Rot G, Curk T, Zupan B, Sugimoto Y, Modic M, Haberman N, Tollervey J, Fujii R, Takumi T, Shaw CE, Ule J (2012) Widespread binding of FUS along nascent RNA regulates alternative splicing in the brain. *Sci Rep* 2: 603

Rossi J, Balthasar N, Olson D, Scott M, Berglund E, Lee CE, Choi MJ, Lauzon D, Lowell BB, Elmquist JK (2011) Melanocortin-4 receptors expressed by cholinergic neurons regulate energy balance and glucose homeostasis. *Cell Metab* 13: 195 – 204

Ruggiu M, Herbst R, Kim N, Jevsek M, Fak JJ, Mann MA, Fischbach G, Burden SJ, Darnell RB (2009) Rescuing Z+ agrin splicing in Nova null mice restores synapse formation and unmasks a physiologic defect in motor neuron firing. *Proc Natl Acad Sci USA* 106: 3513 – 3518

Saxena S, Roselli F, Singh K, Leptien K, Julien JP, Gros-Louis F, Caroni P (2013) Neuroprotection through excitability and mTOR required in ALS motoneurons to delay disease and extend survival. *Neuron* 80: 80 – 96

Schneider CA, Rasband WS, Eliceiri KW (2012) NIH Image to ImageJ: 25 years of image analysis. *Nat Methods* 9: 671 – 675

Schwartz JC, Ebmeier CC, Podell ER, Heimiller J, Taatjes DJ, Cech TR (2012) FUS binds the CTD of RNA polymerase II and regulates its phosphorylation at Ser2. *Genes Dev* 26: 2690 – 2695

Sephton CF, Tang AA, Kulkarni A, West J, Brooks M, Stubblefield JJ, Liu Y, Zhang MQ, Green CB, Huber KM, Huang EJ, Herz J, Yu G (2014) Activity-dependent FUS dysregulation disrupts synaptic homeostasis. *Proc Natl Acad Sci USA* 111: E4769 – E4778

Sheffler-Collins SI, Dalva MB (2012) EphBs: an integral link between synaptic function and synaptopathies. *Trends Neurosci* 35: 293 – 304

Sibley CR, Emmett W, Blazquez L, Faro A, Haberman N, Briese M, Trabzuni D, Ryten M, Weale ME, Hardy J, Modic M, Curk T, Wilson SW, Plagnol V, Ule J (2015) Recursive splicing in long vertebrate genes. *Nature* 521: 371 – 375

Smith BN, Ticozzi N, Fallini C, Gkazi AS, Topp S, Kenna KP, Scotter EL, Kost J, Keagle P, Miller JW, Calini D, Vance C, Danielson EW, Troakes C, Tiloca C, Al-Sarraj S, Lewis EA, King A, Colombrita C, Pensato V *et al* (2014) Exome-wide rare variant analysis identifies TUBA4A mutations associated with familial ALS. *Neuron* 84: 324 – 331

Sonenberg N, Hinnebusch AG (2009) Regulation of translation initiation in eukaryotes: mechanisms and biological targets. *Cell* 136: 731 – 745

Sreedharan J, Blair IP, Tripathi VB, Hu X, Vance C, Rogelj B, Ackerley S, Durnall JC, Williams KL, Buratti E, Baralle F, de Belleroche J, Mitchell JD, Leigh PN, Al-Chalabi A, Miller CC, Nicholson G, Shaw CE (2008) TDP-43 mutations in familial and sporadic amyotrophic lateral sclerosis. *Science* 319: 1668 – 1672

Sun Z, Diaz Z, Fang X, Hart MP, Chesi A, Shorter J, Gitler AD (2011) Molecular determinants and genetic modifiers of aggregation and toxicity for the ALS disease protein FUS/TLS. *PLoS Biol* 9: e1000614

Sun S, Ling SC, Qiu J, Albuquerque CP, Zhou Y, Tokunaga S, Li H, Qiu H, Bui A, Yeo GW, Huang EJ, Eggan K, Zhou H, Fu XD, Lagier-Tourenne C, Cleveland DW (2015) ALS-causative mutations in FUS/TLS confer gain- and loss-of-function by altered association with SMN and U1-snRNP. *Nat Commun* 6: 6171

Tateishi T, Hokonohara T, Yamasaki R, Miura S, Kikuchi H, Iwaki A, Tashiro H, Furuya H, Nagara Y, Ohyagi Y, Nukina N, Iwaki T, Fukumaki Y, Kira JI (2010) Multiple system degeneration with basophilic inclusions in Japanese ALS patients with FUS mutation. *Acta Neuropathol* 119: 355 – 364

Tibshirani M, Tradewell ML, Mattina KR, Minotti S, Yang W, Zhou H, Strong MJ, Hayward LJ, Durham HD (2014) Cytoplasmic sequestration of FUS/TLS associated with ALS alters histone marks through loss of nuclear protein arginine methyltransferase 1. *Hum Mol Genet* 24: 773 – 786

Tollervey JR, Curk T, Rogelj B, Briese M, Cereda M, Kayikci M, Konig J, Hortobagyi T, Nishimura AL, Zupunski V, Patani R, Chandran S, Rot G, Zupan B, Shaw CE, Ule J (2011) Characterizing the RNA targets and position-dependent splicing regulation by TDP-43. *Nat Neurosci* 14: 452 – 458

Trapnell C, Roberts A, Goff L, Pertea G, Kim D, Kelley DR, Pimentel H, Salzberg SL, Rinn JL, Pachter L (2012) Differential gene and transcript expression analysis of RNA-seq experiments with TopHat and Cufflinks. *Nat Protoc* 7: 562 – 578

Tsuiji H, Iguchi Y, Furuya A, Kataoka A, Hatsuta H, Atsuta N, Tanaka F, Hashizume Y, Akatsu H, Murayama S, Sobue G, Yamanaka K (2013) Spliceosome integrity is defective in the motor neuron diseases ALS and SMA. *EMBO Mol Med* 5: 221 – 234

Turgeon B, Meloche S (2009) Interpreting neonatal lethal phenotypes in mouse mutants: insights into gene function and human diseases. *Physiol Rev* 89: 1 – 26

Van Hoecke A, Schoonaert L, Lemmens R, Timmers M, Staats KA, Laird AS, Peeters E, Philips T, Goris A, Dubois B, Andersen PM, Al-Chalabi A, Thijs V, Turnley AM, van Vught PW, Veldink JH, Hardiman O, Van Den Bosch L, Gonzalez-Perez P, Van Damme P *et al* (2012) EPHA4 is a disease modifier of amyotrophic lateral sclerosis in animal models and in humans. *Nat Med* 18: 1418 – 1422

Vance C, Rogelj B, Hortobagyi T, De Vos KJ, Nishimura AL, Sreedharan J, Hu X, Smith B, Ruddy D, Wright P, Ganesalingam J, Williams KL, Tripathi V, Al-Saraj S, Al-Chalabi A, Leigh PN, Blair IP, Nicholson G, de Belleroche J, Gallo JM *et al* (2009) Mutations in FUS, an RNA processing protein, cause familial amyotrophic lateral sclerosis type 6. *Science* 323: 1208 – 1211

Vance C, Scotter EL, Nishimura AL, Troakes C, Mitchell JC, Kathe C, Urwin H, Manser C, Miller CC, Hortobagyi T, Dragunow M, Rogelj B, Shaw CE (2013) ALS mutant FUS disrupts nuclear localisation and sequesters wild-type FUS within cytoplasmic stress granules. *Hum Mol Genet* 22: 2676 – 2688

Waibel S, Neumann M, Rabe M, Meyer T, Ludolph AC (2010) Novel missense and truncating mutations in FUS/TLS in familial ALS. *Neurology* 75: 815 – 817

Waibel S, Neumann M, Rosenbohm A, Birve A, Volk AE, Weishaupt JH, Meyer T, Muller U, Andersen PM, Ludolph AC (2013) Truncating mutations in FUS/TLS give rise to a more aggressive ALS-phenotype than missense mutations: a clinico-genetic study in Germany. *Eur J Neurol* 20: 540 – 546

Wang WY, Pan L, Su SC, Quinn EJ, Sasaki M, Jimenez JC, Mackenzie IR, Huang EJ, Tsai LH (2013) Interaction of FUS and HDAC1 regulates DNA damage response and repair in neurons. *Nat Neurosci* 16: 1383 – 1391

Wegorzewska I, Bell S, Cairns NJ, Miller TM, Baloh RH (2009) TDP-43 mutant transgenic mice develop features of ALS and frontotemporal lobar degeneration. *Proc Natl Acad Sci USA* 106: 18809 – 18814

Yamazaki T, Chen S, Yu Y, Yan B, Haertlein TC, Carrasco MA, Tapia JC, Zhai B, Das R, Lalancette-Hebert M, Sharma A, Chandran S, Sullivan G, Nishimura AL, Shaw CE, Gygi SP, Shneider NA, Maniatis T, Reed R (2012) FUS-SMN protein interactions link the motor neuron diseases ALS and SMA. *Cell Rep* 2: 799 – 806

Yu Y, Chi B, Xia W, Gangopadhyay J, Yamazaki T, Winkelbauer-Hurt ME, Yin S, Eliasse Y, Adams E, Shaw CE, Reed R (2015) U1 snRNP is mislocalized in ALS patient fibroblasts bearing NLS mutations in FUS and is required for motor neuron outgrowth in zebrafish. *Nucleic Acids Res* 43: 3208 – 3218

Zhou Z, Qiu J, Liu W, Zhou Y, Plocinik RM, Li H, Hu Q, Ghosh G, Adams JA, Rosenfeld MG, Fu XD (2012) The Akt-SRPK-SR axis constitutes a major pathway in transducing EGF signaling to regulate alternative splicing in the nucleus. *Mol Cell* 47: 422 – 433

Zhou Y, Liu S, Liu G, Ozturk A, Hicks GG (2013) ALS-associated FUS mutations result in compromised FUS alternative splicing and autoregulation. *PLoS Genet* 9: e1003895

Zou ZY, Cui LY, Sun Q, Li XG, Liu MS, Xu Y, Zhou Y, Yang XZ (2013) *De novo* FUS gene mutations are associated with juvenile-onset sporadic amyotrophic lateral sclerosis in China. *Neurobiol Aging* 34: 1312 e1 – 8